https://doi.org/10.5194/essd-2026-725
Preprint. Discussion started: 18 September 2026

Open Access Earth System Science Data Discussions

A long-term multiscale Critical Zone dataset integrating environmental monitoring and an open-air laboratory: The Alento River Catchment Observatory

Nunzio Romano[1,*], Harry Vereecken[2], Heye R. Bogena[2], Giorgio Cassiani[3], Matteo Censini[3], Giovanna Armiento[4], Marco Proposito[4], Lorenzo De Silvestri[4], Eyal Ben Dor[5], Nicolas Francos[6], Christian Massari[7], János Mészáros[8], Tünde Takáts[8], Caterina Mazzitelli[1], Benedetto Sica[1], Ugo Lazzaro[1], Paolo Nasta[1]

[1] Department of Agricultural Sciences, Division of Agricultural, Forest and Biosystems Engineering, University of Naples Federico II, Portici (Naples), Italy.
[2] Agrosphere Institute, Forschungszentrum Jülich GmbH, Jülich, Germany.
[3] Department of Geosciences, University of Padua, Padova, Italy
[4] Italian National Agency for New Technologies, Energy, and Sustainable Economic Development (ENEA), Sustainability Dept., Roma, Italy.
[5] The Remote Sensing Laboratory, Tel Aviv University, Tel Aviv, Israel.
[6] Sydney Institute of Agriculture & School of Life & Environmental Sciences, The University of Sydney, Sydney, Australia.
[7] IRPI Institute, National Research Council of Italy, Perugia, Italy.
[8] Institute for Soil Sciences, HUN-REN Centre for Agricultural Research, Budapest, Hungary.

Correspondence to: Nunzio Romano (nunzio.romano@unina.it)

Abstract. This paper presents an open-access dataset from the Alento River Catchment (ARC) in southern Italy, a strategic Mediterranean Critical Zone observatory integrating long-term environmental monitoring with an open-air laboratory. Long-term observations of weather variables, streamflow, reservoir water level, groundwater depth, soil water content, and soil matric potential are complemented by targeted field campaigns involving hydrogeophysical surveys, stable water isotope analyses, soil physical and hydraulic measurements, spectral measurements, and high-resolution UAV-based mapping. The principal value of the ARC dataset lies in the coordinated integration of continuous and campaign-based observations across multiple spatial and temporal scales and Critical Zone compartments, providing a basis for linking localized soil and subsurface processes with field- and catchment-scale hydrological responses. Since 2016, the ARC has been a component of the European TERrestrial Environmental Observatories (TERENO) network. The dataset includes both directly measured and derived products, with documented processing procedures, quality-control information, calibration results, and missing-data records. The principal value of the ARC dataset lies in the coordinated integration of continuous and campaign-based observations across multiple spatial and temporal scales and Critical Zone compartments. The combined observations can support the development, calibration, evaluation, and intercomparison of process-based hydrological and Critical Zone models, the evaluation of Earth Observation products, and the investigation of scale-dependent relationships among point-, field-, hillslope-, and catchment-scale observations. The complete dataset is openly accessible through Figshare under a CC BY 4.0 license. (Romano et al., 2026; https://doi.org/10.6084/m9.figshare.31229608).

https://doi.org/10.5194/essd-2026-725
Preprint. Discussion started: 18 September 2026

Keywords: Critical zone, Mediterranean catchment, multi-scale sensor network, cosmic-ray neutron sensor, hydrogeophysics, stable isotopes.

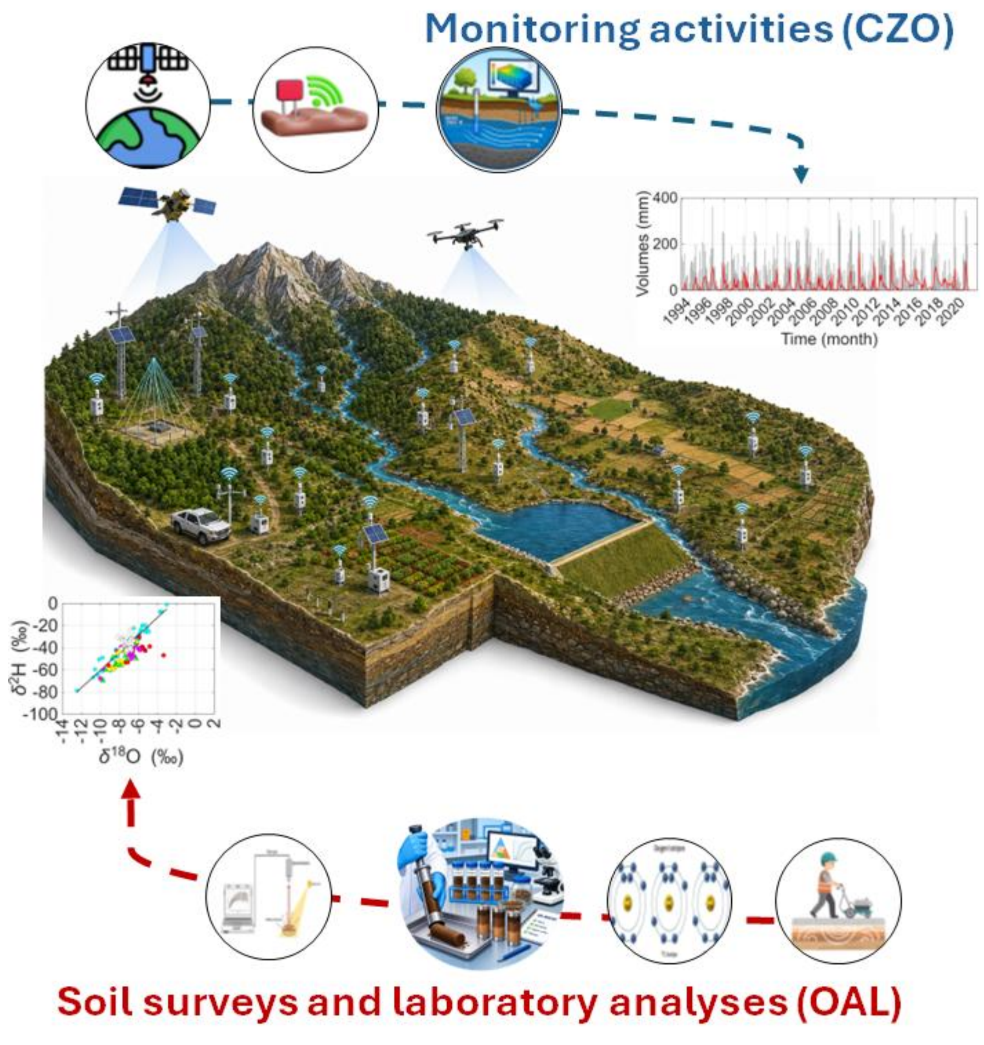

Graphical abstract

https://doi.org/10.5194/essd-2026-725
Preprint. Discussion started: 18 September 2026

1 Introduction

The Critical Zone (CZ) - extending from the vegetation canopy, through the soil, to the groundwater aquifer - is the life-sustaining domain where the hydrological cycle interacts with the lithosphere, biosphere, and atmosphere (Grant and Dietrich, 2017). Characterizing these exchanges enables the identification and quantification of key hydrological processes, including overland flow, infiltration, evapotranspiration, and groundwater flow, that regulate agroecosystem functioning and the provision of services in both natural and managed environments (Brooks et al., 2015). The intricate, nonlinear dynamics of hydrological processes, governed by scale-dependent feedback and spatial-temporal heterogeneity, have stimulated a growing number of programs and initiatives dedicated to establishing environmental observatories. These observatories have advanced scientific understanding while providing the long-term observations needed to support evidence-based management of land and water resources by policymakers, resource managers, and other stakeholders.

Early systematic hydrological monitoring networks were primarily established to collect and disseminate hydrometeorological data. However, these networks soon proved valuable for investigating ecohydrological dynamics and improving understanding of CZ processes. Over the past several decades, the focus has progressively expanded toward CZ observatories designed to investigate the coupled processes controlling water, energy, and solute fluxes across diverse environmental settings. The establishment and long-term sustainability of these observatories, however, depend critically on sustained financial support. To promote harmonized observations and collaborative research, several national and international networks have also been established, including OZCAR in France (Gaillardet et al., 2018), TERENO in Germany (Zacharias et al., 2024) and other European countries, and the Critical Zone Collaborative Network (CZNet) in the USA (Horsburgh et al., 2024). Recent discussions within the Critical Zone community have highlighted the need to identify optimal strategies for designing and maintaining long-term monitoring infrastructures (Nasta et al., 2025). These discussions reflect the need to balance scientific objectives, observational coverage, infrastructure costs, and long-term sustainability. This raises the question of whether greater scientific progress is best achieved through geographically distributed networks of specialized observatories or through a smaller number of comprehensively instrumented research catchments capable of supporting integrated, multidisciplinary investigations (Lappalainen et al., 2025).

The need for long-term, integrated observational data is particularly acute in the Mediterranean region, recognized as one of the global hotspots of climate change and anthropogenic pressure. The region is characterized by strong seasonality, with precipitation temporally decoupled from evapotranspiration: rainfall is concentrated in late fall to early spring, while summers are hot and dry. However, this seasonal pattern is increasingly affected by greater interannual and sub-seasonal variability. Interannual variability is also pronounced, with the duration and timing of wet and dry periods varying substantially among years (e.g., from approximately six wet and six dry months to eight wet and four dry months), thereby complicating water-resource planning (Nasta et al., 2020a). These climatic shifts are compounded by warming-driven changes in the hydrological cycle, which are associated with an increased likelihood of hydrological extremes, including intense short-duration

https://doi.org/10.5194/essd-2026-725
Preprint. Discussion started: 18 September 2026

precipitation and prolonged droughts. Recent IPCC reports warn of increasing seasonal anomalies in the region (Ali et al., 2022).

An equally important challenge for the Mediterranean basin is the impact of land-use changes on the water cycle and sediment transport at catchment and regional scales (Olson et al., 2016). Following World War II, widespread rural abandonment across southern Europe promoted extensive natural reforestation, leading to a substantial expansion of forested areas at the expense of croplands and pastures. In addition, the lack of adequate forest maintenance practices has been identified as a contributing factor to the escalation of wildfire risk (Romano and Ursino, 2020). Farming activities in the Mediterranean region are contingent upon local climatic conditions (Brisson et al., 2010), yet evidence suggests that they are also strongly affected by non-climate drivers, particularly those pertaining to management practices, technological advancements, market prices, and European and national agricultural policies (Bates et al., 2008; Auerswald et al., 2024). These factors may have a more immediate impact on water than those induced by climate change. Nevertheless, during the dry summer months, conflicts often arise between different users (agriculture, tourism, hydropower generation, and drinking water sectors) due to the ever-increasing seasonal water demand. These competing demands highlight the need for scientifically robust information to support public agencies, water authorities, land managers, and private stakeholders in identifying environmentally sensitive areas and prioritizing targeted management interventions.

The Alento River Catchment (ARC) shares similarities with several Mediterranean environments and exhibits features that capture contrasting land-use and geomorphological settings in this region, making it suitable not only as a CZ observatory but also as an open-air laboratory (Romano et al., 2018). The observatory component provides continuous long-term monitoring of environmental variables, enabling the natural dynamics and trends of the agroecosystem to be captured. In contrast, the open-air laboratory supports targeted field campaigns, including intensive and occasionally invasive measurements, designed to quantify agroecosystem properties and processes that cannot be captured through automated monitoring alone. Together, these complementary components provide observations across multiple Critical Zone compartments and spatial and temporal scales. Their integration makes it possible to investigate interactions among atmospheric forcing, vegetation dynamics, soil-water storage, subsurface structure, groundwater, and surface-water response, rather than treating each observation stream independently. The ARC therefore provides an experimental framework in which long-term catchment-scale observations can be interpreted together with spatially distributed and process-specific measurements of the components controlling hydrological response. The dataset addresses the following main themes:

a) Mediterranean climate seasonality and Critical Zone (CZ) functioning; and

b) land-use and land-cover (LULC) change as a driver of agrohydrological dynamics.

These themes are addressed through an integrated observational framework rather than through independent datasets. Atmospheric measurements provide the forcing needed to interpret changes in vegetation, soil-water storage, and catchment water yield; soil moisture and hydraulic observations characterize storage and redistribution; hydrogeophysical measurements provide information on spatially variable subsurface properties; stable isotopes constrain water sources and pathways among precipitation, soil water, groundwater, vegetation, and streams; and surface and groundwater observations provide integrated

https://doi.org/10.5194/essd-2026-725
Preprint. Discussion started: 18 September 2026

responses at the sub-catchment and catchment scales. The resulting combination provides complementary constraints on interactions among Critical Zone components, allowing processes observed at one spatial scale to be evaluated in relation to observations acquired at other scales.

Although numerous environmental observatories have been established worldwide, comparatively few publicly accessible datasets appear to integrate long-term environmental monitoring, multiscale observations, complementary hydrogeophysical and isotopic measurements, and repeated process-oriented field campaigns within a single experimental framework. Most existing datasets emphasize either continuous monitoring or intensive experimentation, whereas the integration of both approaches remains uncommon. The ARC dataset was specifically designed to address this critical need and to help bridge the prevailing gap between the scale of process understanding and the scale of model application by combining continuous observations with targeted experiments that quantify the processes underlying the observed hydrological responses.

Despite the geographical concentration of the observations within a single Mediterranean catchment, the scientific inquiries addressed by the dataset exhibit broad transferability. These include the representation of spatial heterogeneity in environmental models, the transfer of information among observation scales, the identification of water sources and flow pathways, the characterization of soil and subsurface controls on water storage and redistribution, and the assessment of vegetation–water interactions under seasonal water limitation. The value of the ARC dataset for the broader scientific community, therefore, derives from its capacity to provide a well-documented experimental system in which multiple Critical Zone processes can be observed simultaneously, rather than from an assumption that the site is statistically representative of all Mediterranean catchments.

2. Environmental settings and existing gauge network of the Alento River Catchment (ARC)

The Alento River Catchment (ARC; see Fig. 1) encompasses approximately 411 km^2 and is situated within the administrative region of Campania in southern Italy. The catchment area is located within the Cilento, Vallo di Diano, and Alburni National Park, Italy's largest national park, and encompasses landscapes of high ecological value (https://www.cilentoediano.it/). The area includes key water management bodies, such as the Velia Bureau of Irrigation and Land Reclamation (https://www.consorziovelia.com/), and is partially managed by the Alento–Mt. Stella Community Mountain organization (https://www.alento-montestella.sa.it/).

The coastal zone contains settlements including Acciaroli and Pioppi, where human activities such as tourism and traditional agriculture may influence local environmental conditions. General information about the hydrogeological settings and land-use patterns in ARC is available in Romano et al. (2018). The Alento River is a 36 km long river that originates on Mt. Le Corne, at an elevation of 895 m a.s.l. (above sea level), in the Gorga area of the Stio municipality. This river has a typical Mediterranean torrential flow regime, experiencing frequent floods in the fall and severe droughts in the summer, though a minimum flow persists in the dry season. The ARC holds significant strategic value for regional water management. It is anchored by the Piano della Rocca (PdR) earthen dam, the primary and largest structure in a network designed for irrigation, hydroelectric power, and drinking water supply. The ARC is also a site included within the HELP (Hydrology for Environment, Life and Policy) program, which was adopted by UNESCO and WMO in 1999. The biodiversity preserved along the Alento River is highly valuable, leading to the area being recognized as a Site of Community Importance (SCI IT8050012), and forming part of the EU Natura 2000 network under the EU Habitats Directive.

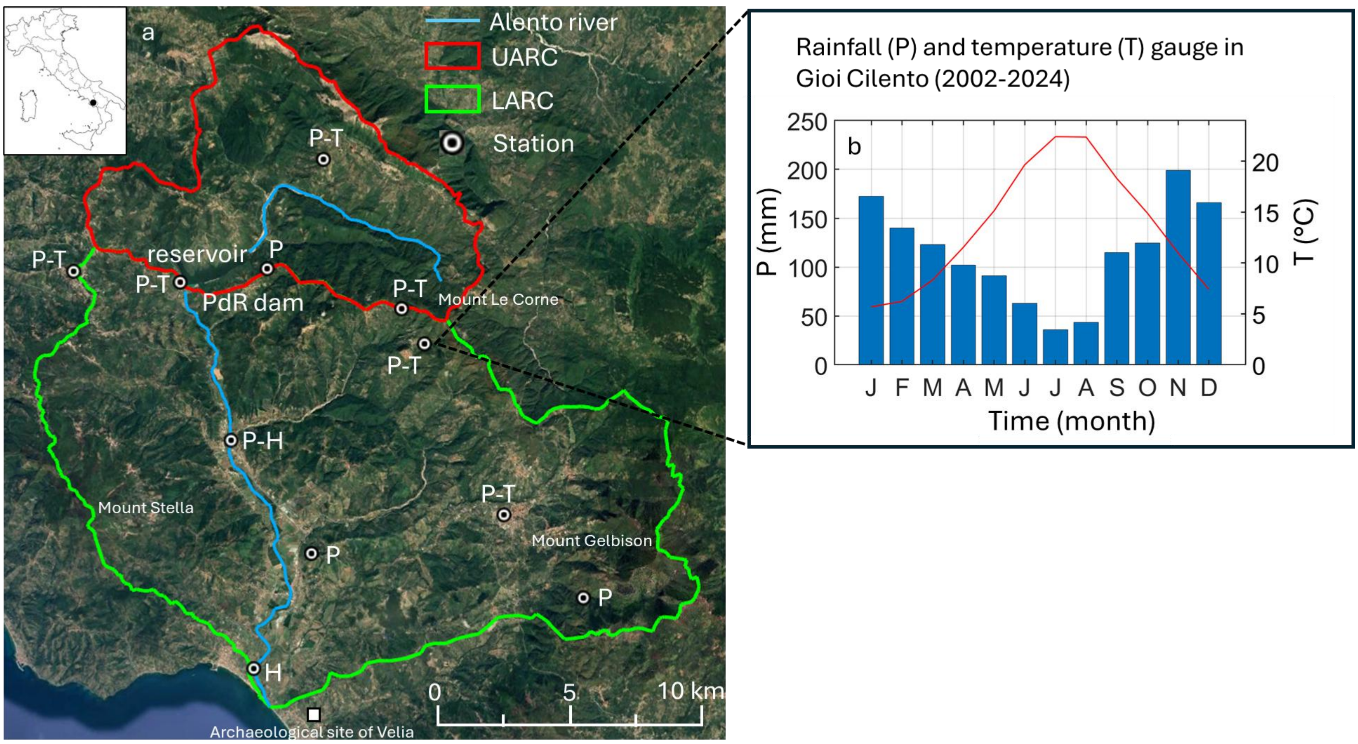

Figure 1: a) the Alento River Catchment (ARC) and the gauge network for measuring rainfall (P), air temperature (T), and the hydrometric water level (H) of the Alento River. The Piano della Rocca earthen dam (PdR dam) separates the drainage boundary of the Upper (UARC) and Lower (LARC) ARC; b) mean monthly rainfall (blue bars) and air temperature (red line) at the Gioi Cilento weather station, obtained from daily data monitored in the period between 2002 and 2024.

According to the Köppen-Geiger classification, the climate in this area is categorized as Csa (warm temperate climate with hot-dry summer; Peel et al., 2007) and is generally characterized by hot-dry summers and mild-wet winters (Nasta et al., 2020b). The management of water resources within the ARC is significantly shaped by the Mediterranean climate seasonality (Kutiel and Trigo, 2014). While inhabitants across the Mediterranean region have historically adapted to these conditions since ancient times through traditional water management, the socio-economic shifts of the last century have generated novel complexities and challenges. Consequently, the ARC represents an interesting research area for the optimal management of water resources within a river basin by using a supply-side and a demand-side approach (Ellison et al., 2012; Nasta et al., 2017). Water demand in the ARC is rising during summer not only because of increased farming needs, but also in response to an unprecedented seasonal tourist influx, particularly in coastal areas. In addition to the seasonal mismatch between water

https://doi.org/10.5194/essd-2026-725
Preprint. Discussion started: 18 September 2026

availability and water demand, there is also a pronounced spatial mismatch between water production in the mountainous headwaters and water use in the downstream agricultural and coastal areas. According to the IPCC report (2022), environmental challenges in the region are projected to intensify as the Mediterranean climate shifts toward hotter and more extreme hydroclimatic conditions. Whereas rising average temperatures and increasing precipitation variability may not necessarily significantly alter total annual rainfall amounts, they are expected to drive a higher frequency of intense, short-duration storm events and more persistent droughts. These shifting patterns heighten the risk exposure to key local crops, particularly vineyards, olive groves, and deciduous fruit orchards (Nasta et al., 2013). The precipitation (P), air temperature (T), and hydrometric water-level (H) observations collected by the regional gauge network listed in Table 1 are publicly available through the Campania Region Functional Centre (Centro Funzionale Multirischi della Regione Campania) data portal (https://centrofunzionale.regione.campania.it/dati).

Table 1. Precipitation (P), air temperature (T), and hydrometric water-level (H) gauge stations within the ARC.

Easting m	Northing m	Elevation m (a.s.l.)	Sensor	Name of the station
511871	4447171	10	H	Chiusura Alento
519299	4460300	699	P-T	Gioi Cilento
504968	4463551	420	P-T	Torchiara
511140	4456545	43	P-H	Omignano Scalo
522341	4453306	377	P-T	Vallo della Lucania
514392	4451861	180	P	Vallo Scalo
512878	4463501	417	P	Perito-Ostigliano
525534	4449911	617	P	Ceraso-Vivaio Isca
515273	4467891	400	P-T	MFC2
518407	4461734	710	P-T	GOR1
509213	4463050	110	P-T	Dam Alento

The ARC can be divided into two distinct topographical zones based on their position relative to the PdR dam: 1) the upstream zone (referred to as the Upper Alento River Catchment, or UARC) covers approximately 102 km^2 and is predominantly characterized by hilly and mountainous landscapes, and 2) the downstream zone (referred to as the Lower Alento River Catchment, or LARC) covers approximately 309 km^2 and consists of hills and valleys sloping toward the Tyrrhenian Sea with prevalence of agricultural lands and livestock farming. This system is managed by the Velia Bureau of Irrigation and Reclamation. The distinction between ARC, UARC, and LARC is maintained throughout the manuscript because the spatial support of the observations and derived hydrological products differs among these spatial domains.

3. The monitoring infrastructure in LARC

3.1 Alento River hydrometric level at LARC outlet

As part of the hydraulic and hydrological monitoring program launched in 1920, the Italian Hydrological Service established a hydrometric station on the Alento River near the town of Casalvelino Scalo in 1958. This station is located close to the river mouth (X=511,871.00 m, Y=4,447,171.00 m), at an elevation of about 10 m above sea level. However, the record of river hydrometric water levels is not continuous over the entire monitoring period, and conversion of stage observations to discharge has also been constrained by the availability and stability of stage-discharge relationships. Despite these limitations, the long-term stage record provides an invaluable historical reference for assessing hydrological variability within the catchment up to the present day.

3.2 Water reservoir hydrometric water-level and water yield at Piano della Rocca dam

To address not only the recurring water crises, typical of the Mediterranean region, but also to promote socioeconomic growth in inland areas, which were further disadvantaged by the migration to cities during the 1960s, the Piano della Rocca (PdR) earthen dam was constructed and began operations in 1996. The PdR dam, which also serves flood control, represents the largest and most important component of an interconnected hydraulic system designed to store and distribute the catchment's water resources to various users, but primarily for irrigation purposes. The PdR dam can be seen as a link between the Upper ARC, the most mountainous and forested part of the basin, and the Lower ARC, which slopes towards the sea and features a greater prevalence of agricultural lands and livestock farming. This system is managed by the Velia Bureau of Irrigation and Reclamation.

Water stored in the artificial lake is exploited for the following purposes: irrigation (32%), industrial water supply and hydroelectric power (24%), drinking water (21%), environmental flows (18%), and non-drinking water (5%). The reservoir is located at an average elevation of approximately 110 meters above sea level (a.s.l.) and has a maximum water volume of approximately 28 million cubic meters. The maximum surface area of the artificial lake is approximately 2 km^2, whereas the maximum depth is approximately 30 meters. The Velia Bureau for Land Reclamation and Irrigation is responsible for monitoring the water level, as well as managing the reservoir water volumes for different uses. A weather station was deployed near the dam to record daily precipitation (P) (see Fig. 2a) and reference evapotranspiration (ET_0). The dam's reservoir water balance dictates that the variation over time of the water volume (V) accumulated inside the reservoir is given by the difference between the incoming (Q_{in}) and outgoing (Q_{out}) flow rates:

$$\frac{dV}{dt} = Q(t)_{in} - Q(t)_{out} \quad (1).$$

While the reservoir's water volume (V) and the outgoing flow rate (Q_{out}) are monitored, the reservoir water balance was used to estimate the daily catchment inflow rate (Q_{in}) through Eq.(1) because direct measurements of Q_{in} were not available. Direct precipitation on the reservoir surface was not explicitly included in Eq. (1); its contribution is expected to be small relative to catchment inflow but should be considered when interpreting the derived water-yield product. Volume V (in m^3) is derived from the reservoir volume curve based on the daily hydrometric water-levels (WL, in m) recorded by an ultrasonic level meter installed at the intake structure of the dam (see Fig. 2b). Daily reservoir water levels (ranging between 90.0 m and 119.3 m) measured at the PdR dam were converted into reservoir storage V using the following empirical storage-elevation relationship:

$$V = 2.90 \cdot 10^4 \times WL^2 - 5.11 \cdot 10^6 \times WL + 2.26 \cdot 10^8 \quad (2).$$

Because catchment inflow is derived indirectly from the reservoir water balance, the resulting water-yield product inherits uncertainties associated with reservoir storage estimation, the stage–storage relationship, outgoing discharge, leakage, evaporation losses, and the omission of direct precipitation on the reservoir surface. The water-yield series should therefore be regarded as a derived catchment-scale hydrological product rather than as a direct measurement of streamflow.

Periods during which the reservoir level exceeded the spillway elevation (118 m a.s.l.) are identified as overflow events (marked with a horizontal dashed line in Fig. 2b). The time series clearly shows the recurrent pattern of the reservoir filling during the wet season and the subsequent draw-down during the summer months due to water demands. The periods of overflow (cyan circles) are generally clustered in the wet winter/spring seasons. Q_{out} is given by the summation of surface and bottom discharge, leakage through the weir, and evaporation losses from the liquid surface. The estimated daily inflow Q_{in} (in m^3 d^{-1}) was converted to catchment-equivalent water yield (WY, in mm d^{-1}) by dividing by the drainage area of UARC and converting the resulting water depth from meters to millimeters. Monthly water yield was then calculated by summing the daily values and compared with monthly precipitation (see Fig. 2c). Figure 2c highlights the seasonal variability in the area and shows that the highest WY typically occurs during the wettest months following the concentrated rainfall. Because WY is a derived quantity, it should not be interpreted as a direct streamflow measurement. All variables are reported using SI units and accompanied by standardized timestamps.

https://doi.org/10.5194/essd-2026-725
Preprint. Discussion started: 18 September 2026

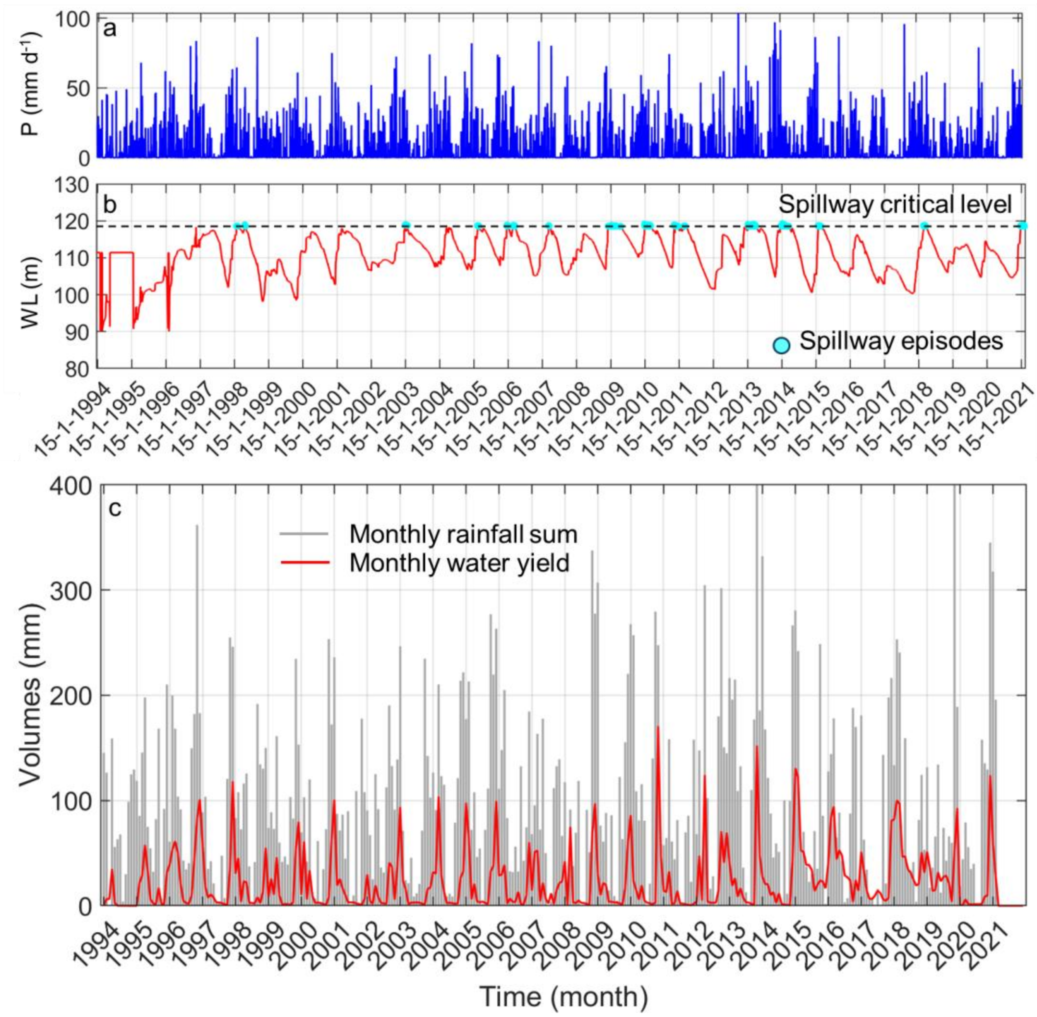

Figure 2: Time series of a) daily rainfall (P) recorded at the weather station deployed near the Piano della Rocca dam, b) daily water level (WL, red line) recorded in the reservoir with overflow episodes (cyan circles) surpassing the critical overflow level of 118 m (shown as horizontal dashed line), c) monthly sums of rainfall (P, grey bars) and water yield (WY, red line) in the same recording time (1994-2021).

4. Experimental sites and monitoring infrastructures in UARC

Considering the strategic importance of the water resources stored in the reservoir impounded by the PdR dam, a series of investigations were initiated in the early 2000s, primarily to improve the understanding of the geology, landscape settings, soil type and vegetation, and hydrology of UARC (Romano et al., 2018). Research activities began in the UARC in 2005 by organizing a pedological survey to generate a soil-landscape unit map. A field campaign was carried out by collecting 105 soil samples across six distinct transects to determine soil physical, chemical, and hydraulic properties (Nasta et al., 2018). The outcomes of these studies supported the establishment of some monitoring sub-catchments designed to collect targeted data,

https://doi.org/10.5194/essd-2026-725
Preprint. Discussion started: 18 September 2026

enabling the hydrological responses to be identified under contrasting geomorphological, pedological, and vegetation conditions. Three experimental sub-catchments (MFC1, MFC2, and GOR1) were established to combine continuous monitoring with field surveys (see Fig. 3).

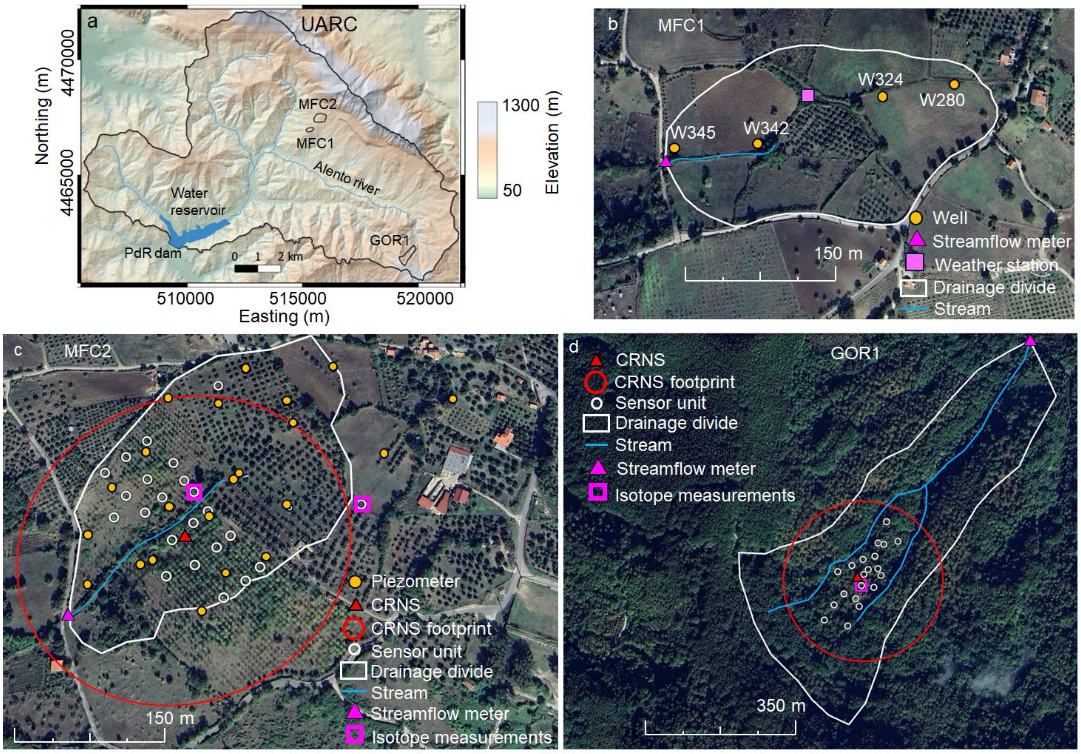

Figure 3: a) Locations of the MFC1, MFC2, and GOR1 experimental sites within the UARC represented through a 5-m Digital Elevation Model (DEM); b) monitoring infrastructure at MFC1; c) monitoring infrastructure at MFC2, including the streamflow meter, wireless sensor network, Cosmic Ray Neutron Sensor (CRNS) and its nominal footprint (red circle with a 180-m radius), piezometer network, and isotope measurement plots; d) monitoring infrastructure at GOR1, including the streamflow meter, wireless sensor network, Cosmic Ray Neutron Sensor (CRNS) and its nominal footprint (red circle with 180 m radius), and isotope measurement plot.

The experimental sites established within the UARC constitute the operational core of the open-air laboratory component of the ARC. Unlike conventional monitoring stations that primarily record environmental variables, these sites were specifically designed to support hypothesis-driven experiments aimed at understanding the mechanisms controlling water storage, flow, and transport within the Mediterranean Critical Zone. Continuous observations are therefore complemented by repeated field campaigns that characterize subsurface properties, soil hydraulic response, geophysical signatures, isotope dynamics, and surface morphology.

The monitoring sites described below should be regarded as nested observation domains within the ARC rather than as independent datasets. LARC provides catchment-scale hydrological observations, whereas MFC1, MFC2, and GOR1 provide progressively more detailed observations of selected soil, vegetation, subsurface, and hydrological processes. The scientific value of the combined dataset is derived from its capacity to establish connections between these observations across diverse locations and dimensions.

4.1 The MFC1 site

The MFC1 experimental site was established to investigate hillslope-scale hydrological processes in a Mediterranean agricultural landscape characterized by gently sloping south-facing terrain cultivated with annual crops and sparsely distributed cherry and olive trees growing on predominantly clayey soils.

Between 2006 and 2009, the site was equipped to monitor the main components of the local water balance. Continuous observations included daily precipitation (P), reference crop evapotranspiration (ET_0), streamflow (Q) at the catchment outlet, and depth to groundwater in four harvesting cased stone-lined wells (W280, W324, W342, and W345). Soil water content (θ) was measured during thirteen field campaigns using a portable time-domain reflectometer.

The resulting dataset combines meteorological forcing, streamflow, groundwater dynamics, and spatial soil moisture surveys within a single experimental catchment (Nasta et al., 2013). These measurements provide a valuable benchmark for investigating runoff generation mechanisms and the scaling of hydrological processes from point measurements to the hillslope scale.

4.1.1 Weather data

An automatic weather station installed at the MFC1 experimental site (400 m a.s.l.) continuously monitored the main meteorological variables controlling the local water balance. The station recorded precipitation (P), air temperature, relative humidity, wind speed and direction, and the four components of the radiation balance using an NR01 four-component net radiometer (Hukseflux Thermal Sensors, Delft, The Netherlands). Meteorological variables were recorded at hourly intervals. Following the recommendations of the World Meteorological Organization (WMO), air temperature and wind speed were measured at a height of 3.0 m, whereas the radiometers were installed 2.0 m above the soil surface. Daily reference evapotranspiration (ET_0) was calculated from the hourly meteorological observations using the FAO Penman–Monteith equation (Allen et al., 1998; Batsukh et al., 2021). Both P and ET_0 are provided in the repository as daily aggregated values.

Quality assurance procedures included routine inspection of the time series to identify physically unrealistic values and periods affected by instrument malfunction, data logger interruptions, power supply failures, or communication problems.

4.1.2 Campaign-based manual soil water content

Apparent dielectric bulk permittivity, K_b (unitless), was measured during thirteen field campaigns conducted between 1 September 2006 and 24 April 2008 using a portable time-domain reflectometer (TDR; Tektronix 1502B/C) equipped with a custom three-rod probe (rod length of 15 cm). Measurements were collected at 112 predefined sampling locations distributed

https://doi.org/10.5194/essd-2026-725
Preprint. Discussion started: 18 September 2026

throughout the MFC1 experimental catchment. Volumetric soil water content (θ, cm³ cm⁻³) was estimated from the measured dielectric permittivity using the universal third-order calibration equation proposed by Topp et al. (1980):

$$\theta = 4.3 \cdot 10^{-6} \times K_b^3 - 5.5 \cdot 10^{-4} \times K_b^2 + 2.92 \cdot 10^{-2} \times K_b - 5.3 \cdot 10^{-2} \quad (3).$$

Approximately 33% of the scheduled measurements are missing. These missing observations are largely attributable to the practical limitations inherent in conducting repeated manual TDR surveys under Mediterranean field conditions, rather than to sensor malfunction. During the dry summer period, the clay-rich soil became extremely hard and developed extensive shrinkage cracks, while the presence of coarse fragments frequently prevented complete insertion of the TDR rods or caused mechanical damage to the probe. In addition, rapid seasonal vegetation growth, including dense grasses, thorny shrubs, and brambles, rendered several sampling locations inaccessible during late spring and summer field campaigns. To preserve the integrity of the original observations, no gap-filling or interpolation procedures were applied, and missing measurements are explicitly identified in the dataset using standard missing-value flags. Before each field campaign, the TDR instrument was checked following the manufacturer's recommendations. Measurements showing incomplete rod insertion, unstable waveforms, or obvious acquisition errors were discarded. The dataset contains only validated observations, while unsuccessful measurements are reported as missing values without interpolation.

4.1.3 Streamflow and depth to groundwater measurements

Streamflow (Q) at the MFC1 experimental catchment was monitored continuously by measuring the water level upstream of a 90° V-notch weir installed at the catchment outlet. Water level was recorded at 10-min intervals and converted to stream discharge using the stage–discharge relationship established for the weir. Groundwater dynamics were monitored continuously in four hand-dug, stone-lined wells (W280, W324, W342, and W345) distributed across the catchment. The depth to the groundwater table was recorded every 10 min using Odyssey capacitance-type water-level loggers (Dataflow Systems Pty Ltd., Australia; https://odysseydatarecording.com/).
Quality assurance procedures included routine inspection of the time series to identify anomalous measurements associated with sensor maintenance, temporary logger malfunction, or periods when water levels fell outside the measurement range of the instruments. Missing observations were retained as missing values, and no gap-filling or interpolation procedures were applied.

4.2 The MFC2 and GOR1 sites

The MFC2 and GOR1 experimental sites were established to investigate Critical Zone processes under contrasting Mediterranean land-use and geomorphological settings while maintaining a common monitoring strategy. MFC2 is an approximately 8 ha agricultural catchment characterized predominantly by clay and clay-loam soils, whereas GOR1 is an approximately 18 ha forested catchment located on a steep north-facing hillslope with predominantly loamy soils (Nasta et al.,

https://doi.org/10.5194/essd-2026-725
Preprint. Discussion started: 18 September 2026

2020b). Together, the two sites provide complementary observations representative of managed and natural ecosystems within the Upper Alento River Catchment (UARC).

To facilitate direct comparisons of hydrological responses, both sites were instrumented following the same experimental design. Since 2016, each site has operated an automatic weather station, a wireless sensor network (SoilNet, Forschungszentrum Jülich, Germany) consisting of twenty monitoring locations equipped with GS3 and MPS-6 sensors installed at depths of 15 and 30 cm, and a stationary Cosmic-Ray Neutron Sensor (CRNS). Both CRNS stations are part of the COSMOS-Europe network (Bogena et al., 2022). Long-term monitoring is complemented by repeated hydrogeophysical surveys and stable water isotope sampling campaigns. Targeted field campaigns for measuring soil physical and hydraulic properties and soil spectral characteristics were conducted only at MFC2.

4.2.1 Weather data

Automatic weather stations have been installed at the MFC2 (400 m a.s.l.) and GOR1 (711 m a.s.l.) experimental sites. The MFC2 station is the same station used for the nearby MFC1 site due to their close proximity. Both stations are equipped with identical sensors and continuously record precipitation (P), air temperature, relative humidity, wind speed and direction, and the four components of the radiation balance using an NR01 four-component net radiometer (Hukseflux Thermal Sensors, Delft, The Netherlands). Meteorological variables are recorded at hourly intervals.

Following the recommendations of the World Meteorological Organization (WMO), air temperature and wind speed are measured at a height of 3.0 m, whereas the radiometers are installed 2.0 m above the soil surface. Daily reference evapotranspiration (ET_0) was calculated from the hourly meteorological observations using the FAO Penman–Monteith equation (Allen et al., 1998; Batsukh et al., 2021). Both precipitation and ET_0 are provided in the repository as daily aggregated values.

Quality assurance procedures included routine inspection of the time series to identify physically unrealistic values and periods affected by instrument malfunction, data logger interruptions, power supply failures, or communication problems. Approximately 1.3% and 2.4% of the meteorological records are missing at the MFC2 and GOR1 weather stations, respectively. To preserve the integrity of the original observations, no gap-filling or interpolation procedures were applied, and all missing records are explicitly identified using standard missing-value flags.

4.2.2 CRNS-based area-wide soil moisture

Field-scale soil moisture was monitored continuously at the MFC2 and GOR1 experimental sites using stationary CRS-2000/B Cosmic-Ray Neutron Sensors (Hydroinnova LLC, Albuquerque, USA). Each detector employs a $^{10}BF_3$ proportional counter to measure epithermal neutron intensity at 15 min intervals. Each station is equipped with auxiliary sensors measuring air temperature, relative humidity, and atmospheric pressure, which are required to correct the raw neutron count rates for atmospheric effects.

https://doi.org/10.5194/essd-2026-725
Preprint. Discussion started: 18 September 2026

Raw neutron counts were processed using a dedicated MATLAB workflow that (*i*) screened and removed anomalous observations, (*ii*) aggregated the observations to hourly and daily values, (iii) corrected neutron counts for variations in atmospheric pressure, air humidity, and incoming cosmic-ray intensity, and (iv) applied a temporal smoothing procedure to reduce high-frequency counting noise. Variations in incoming cosmic-ray intensity were corrected using observations from the Jungfraujoch neutron monitor (JUNG, Switzerland) following Zreda et al. (2012), whereas atmospheric water-vapor corrections followed Rosolem et al. (2013). The repository contains volumetric soil moisture estimates derived from corrected neutron count rates using both the revised standard N_0 transfer function of Desilets et al. (2010) and the Universal Transport Solution (UTS) of Köhli et al. (2021).

Site-specific calibration was performed following Heidbüchel et al. (2016) using three independent field sampling campaigns conducted under dry, intermediate, and wet soil conditions. During each campaign, soil samples were collected at 18 locations surrounding the CRNS, with six sampling points positioned at radial distances of 1, 33, and 140 m. At each location, a split-tube sampler was used to extract a 30 cm long soil core into a plastic liner. Each core was subsequently divided into six 5 cm sections, resulting in a total of 108 soil samples per campaign (18 locations × 6 depth increments). Volumetric soil water content, bulk density, soil organic matter, and lattice water were determined using standard laboratory procedures and used to calibrate the site-specific calibration parameter (N_0). Following calibration, the CRNS-based soil moisture estimates achieved a root mean square error (RMSE) of approximately 0.019 $cm^3\ cm^{-3}$ at MFC2 and 0.034 $cm^3\ cm^{-3}$ at GOR1 relative to an independent set of field observations. The repository provides daily aggregated field-scale volumetric soil-water content derived from the calibrated CRNS observations. Quality assurance procedures included automated screening of unrealistic neutron counts, atmospheric corrections, removal of outliers, and routine inspection of the processed time series. Data gaps resulting from power outages, battery depletion, data logger malfunction, or instrument maintenance are reported as missing values and account for 16.4% and 22.3% of the CRNS records at MFC2 and GOR1, respectively. No gap-filling or interpolation procedures were applied, and missing observations are explicitly identified using standard missing-value flags.

An important feature of the ARC dataset is the temporal and spatial overlap among observations obtained with different techniques. This overlap provides opportunities for cross-validation and consistency assessment across observation scales. For example, CRNS-based field-scale soil-water content can be compared with spatially distributed SoilNet and campaign-based TDR measurements, while EMI and ERT surveys provide complementary information on the spatial distribution and subsurface organization of soil-water conditions. Stable water isotope observations provide an independent process-based constraint on water sources and flow pathways. Such cross-technique comparisons allow users to evaluate the consistency, scale dependence, and limitations of individual observations rather than interpreting each data stream independently.

4.2.3 Continuous soil water content and soil matric potential profiles

At both the MFC2 and GOR1 sites, twenty monitoring locations were instrumented with GS3 and MPS-6 sensors (METER Group Inc., Pullman, WA, USA) installed at soil depths of 15 and 30 cm. The GS3 sensors continuously measured apparent

https://doi.org/10.5194/essd-2026-725
Preprint. Discussion started: 18 September 2026

bulk dielectric permittivity (K_b, dimensionless), soil temperature (T, °C), and bulk electrical conductivity (EC_b, mS cm^{-1}), whereas the MPS-6 sensors monitored soil matric potential (h, kPa). All variables were recorded at 15 min intervals.

Volumetric soil water content (θ, cm^3 cm^{-3}) was estimated from the measured dielectric permittivity using site-specific, temperature-corrected calibration equations developed for the two experimental sites (Nasta et al., 2024). For MFC2, soil water content was calculated as:

$$\theta = (-0.0012\,T + 0.1597)\sqrt{K_b} + (0.0028\,T - 0.2992) \quad (4),$$

while for GOR1:

$$\theta = (0.0014\,T + 0.1875)\sqrt{K_b} + (-0.0053\,T - 0.4370) \quad (5).$$

The calibration yielded root mean square errors (RMSE) of 0.019 cm^3 cm^{-3} (1.9%) at MFC2 and 0.007 cm^3 cm^{-3} (0.7%) at GOR1. These calibrated volumetric soil water contents are the values distributed in the repository.

Apparent dielectric bulk permittivity, K_b (unitless), was measured during nineteen and sixteen field campaigns in MFC2 and GOR1, respectively, conducted between October 2018 and December 2021 using a portable time-domain reflectometer (TDR; Tektronix 1502B/C) equipped with a custom three-rod probe (rod length of 15 cm). Measurements were collected over the topsoil at the 20 SoilNet unit positions. Volumetric soil water content (θ, cm^3 cm^{-3}) was estimated from the measured dielectric permittivity using the universal third-order calibration equation proposed by Topp et al. (1980).

The MPS-6 sensors operate within a matric potential range of approximately −91.8 to −1070.7 cm. Consequently, soil matric potential is not reported during periods when soils are close to saturation because measurements fall outside the operating range of the sensors.

Quality assurance procedures included automatic screening of physically unrealistic values, verification of sensor consistency, and routine inspection of the time series. Missing observations resulted primarily from temporary power outages, data logger interruptions, communication failures, and occasional damage to cables and sensors caused by wildlife, particularly wild boars digging around the monitoring stations and other animals damaging exposed wiring. To preserve the integrity of the original observations, no gap-filling or interpolation procedures were applied, and all missing records are explicitly identified using standard missing-value flags.

Within the integrated ARC framework, these observations provide point-scale information on soil-water dynamics that can be related to catchment meteorological forcing and to larger-support observations from CRNS and spatial hydrogeophysical surveys.

4.2.4 Hydrogeophysical observations

Repeated hydrogeophysical surveys were conducted at the MFC2 and GOR1 experimental sites to complement the continuous point-scale observations provided by the sensor networks with spatially distributed information on subsurface electrical

https://doi.org/10.5194/essd-2026-725
Preprint. Discussion started: 18 September 2026

properties. The repository includes both electromagnetic induction (EMI) and electrical resistivity tomography (ERT) datasets collected between August 2020 and December 2021.

EMI surveys were performed using a GEM-2 SKI multifrequency electromagnetic sensor (Geophex Ltd., USA) operated in the horizontal coplanar (HCP) configuration with an intercoil spacing of 1.66 m. Apparent electrical conductivity was measured simultaneously at six operating frequencies (425, 1,525, 5,325, 18,325, 63,025, and 92,775 Hz). Because the effective depth of investigation depends on frequency as well as subsurface electrical properties, the multifrequency observations provide sensitivity to subsurface depths of approximately 3 m. A total of seven field campaigns were conducted under contrasting seasonal soil moisture conditions. The repository contains both the raw multifrequency apparent electrical conductivity measurements and the inverted electrical conductivity profiles obtained using EMagPy (McLachlan et al., 2021). Each survey includes acquisition date, measurement coordinates, operating frequency, inversion results, and associated metadata. These observations can be used to characterize the spatial variability of soil moisture, texture, and subsurface heterogeneity and to support hydrological model parameterization. High-resolution ERT surveys were conducted within the same experimental areas using a dipole–dipole acquisition array with 1 m electrode spacing. Reciprocal measurements were acquired during every survey following Cassiani et al. (2006) to quantify measurement uncertainty and provide an independent quality assessment of the electrical data.

The repository includes electrode coordinates, acquisition geometry, apparent resistivity measurements, reciprocal errors, and inverted resistivity sections obtained using the R2 inversion algorithm implemented in ResIPy (Blanchy et al., 2020). The inverted products provide detailed information on subsurface architecture and its temporal variability and are suitable for investigating soil water redistribution, preferential flow pathways, groundwater occurrence, and Critical Zone processes.

Quality assurance included verification of GPS positioning, screening and removal of measurements exceeding the predefined reciprocal error threshold, inspection of inversion residuals, and consistency checks among repeated surveys. Missing observations mainly reflect field conditions that prevented data acquisition, including flooded terrain, inaccessible locations, or instrument maintenance. No gap-filling or interpolation procedures were applied, and unavailable surveys are explicitly identified in the repository.

The hydrogeophysical observations provide a spatial bridge between localized soil and groundwater measurements and the larger-scale hydrological response of the experimental catchments. EMI and ERT surveys are utilized to characterize spatial patterns in subsurface electrical properties. These patterns can be interpreted in conjunction with soil moisture, soil hydraulic properties, topography, groundwater observations, and hydrological response. The aforementioned subjects make two primary contributions to the integrated dataset. Firstly, a set of subsurface measurements has been made available. Secondly, they have demonstrated the possibility of relating spatial heterogeneity to hydrological processes across different observation scales.

The integration of continuous hydrological monitoring with repeated hydrogeophysical imaging enables users to investigate not only temporal variations in water storage but also the evolving spatial organization of subsurface processes. This combination substantially increases the usefulness of the dataset for hydrological model parameterization, structural validation, and process interpretation. Moreover, when interpreted together with the co-located SoilNet and CRNS observations, the

https://doi.org/10.5194/essd-2026-725
Preprint. Discussion started: 18 September 2026

hydrogeophysical surveys provide an opportunity to assess how spatially distributed subsurface information relates to point- and field-scale measurements of soil-water dynamics.

4.2.5 Isotope measurements

Stable water isotope observations comprise measurements of δ²H and δ¹⁸O collected approximately every two weeks from rainfall, soil water, stream water, groundwater, and xylem water to characterize water sources and transport processes within the Critical Zone.

Sampling campaigns were conducted from 1 October 2020 to 31 October 2022 at both experimental sites. Representative sampling plots were established adjacent to SoilNet Unit 4 beneath a downy oak (*Quercus pubescens*) at MFC2 and SoilNet Unit 13 beneath a chestnut (*Castanea sativa*) at GOR1. Rainfall was collected using Palmex rain collectors (Palmex Ltd., Zagreb, Croatia) installed near the automatic weather stations.

Soil samples were collected at depths of 15 cm, 30 cm, and 100 cm, with three replicates per sampling depth. Xylem water was obtained from bark-free twigs collected from representative trees, while stream water samples were collected concurrently. Groundwater samples were collected only in MFC2. Soil and plant samples were stored in airtight 12 mL Exetainer vials, transported under refrigerated conditions, and processed at the C.I.R.Ce. laboratory (University of Campania "Luigi Vanvitelli"). Water was extracted by cryogenic vacuum distillation, and isotope ratios were determined using Isotope Ratio Mass Spectrometry (IRMS). Isotopic compositions are reported in standard ‰ notation relative to Vienna Standard Mean Ocean Water (VSMOW). The repository provides the average value of the three field replicates for each sampling date, together with sampling location, water compartment, sampling depth, δ²H, and δ¹⁸O. Figure 4 illustrates the dual-isotope composition (δ²H and δ¹⁸O) of the principal water compartments sampled at the MFC2 and GOR1 experimental sites. Rainfall, stream water, and groundwater generally plot close to the Local Meteoric Water Line (LMWL), whereas soil water exhibits progressive isotopic enrichment relative to the LMWL, particularly in the shallow soil layers, reflecting evaporative fractionation. Xylem-water isotopic compositions overlap substantially with those of soil water, providing a basis for investigating potential source-water and root-water uptake. Concurrent collection of isotope observations with hydrometeorological, soil moisture, hydrogeophysical, and groundwater measurements enables integrated analyses of water sources, travel times, root-water uptake, and subsurface flow pathways. Such analyses would not be feasible by employing a singular observation technique in isolation. Quality assurance included replicate sampling, laboratory reference standards, and routine verification of analytical precision throughout the monitoring period. Missing observations occur for two main reasons. First, xylem samples were intentionally not collected during the winter dormant season, when trees were leafless and transpiration was negligible. Second, several δ²H analyses are unavailable because the IRMS facility was temporarily out of service for an extended period. To preserve the integrity of the original observations, no gap-filling or interpolation procedures were applied, and all missing records are explicitly identified using standard missing-value flags. Potential uncertainties

https://doi.org/10.5194/essd-2026-725
Preprint. Discussion started: 18 September 2026

associated with water extraction, including matrix-dependent extraction efficiency and possible isotope fractionation, should be considered when comparing isotope compositions among water compartments.

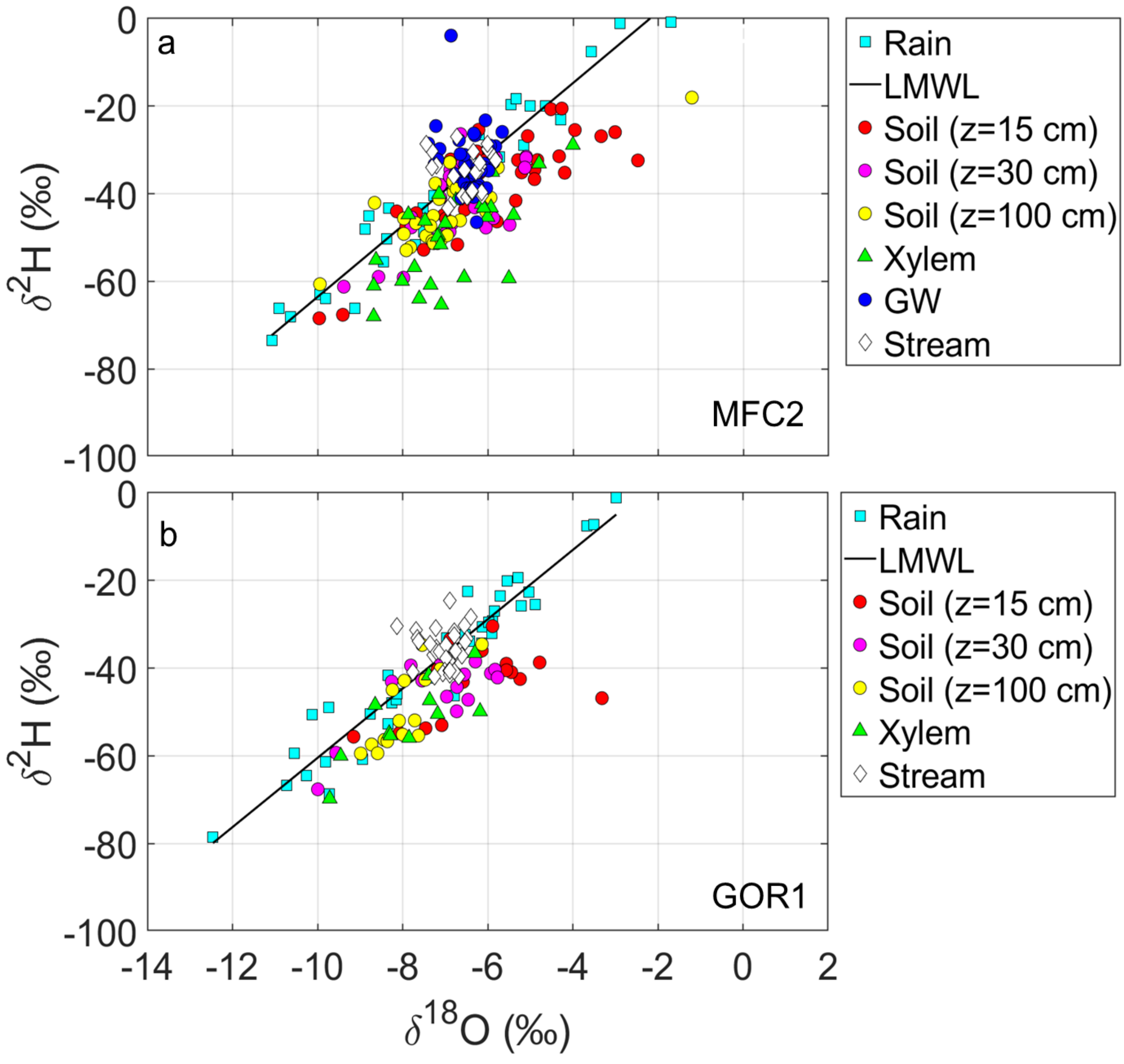

500 **Figure 4: Dual isotope plot of hydrogen and oxygen stable isotopes (δ^2H and δ^{18}O) for the main water types (i.e., rain, groundwater, stream) at soil depths of 15 cm, 30 cm, and 100 cm, as well as xylem, at a) MFC2 and b) GOR1. The black solid line depicts the local meteoric water line (LMWL).**

The isotope dataset establishes a critical link between multiple Critical Zone compartments at the process level. When combined with hydrometeorological, soil-moisture, groundwater, and streamflow observations, the isotope measurements can be used to investigate water sources, mixing, storage, travel times, and transport pathways connecting precipitation, soil water,

https://doi.org/10.5194/essd-2026-725
Preprint. Discussion started: 18 September 2026

groundwater, vegetation, and streams. This cross-compartment integration provides information that cannot be obtained from any individual observation technique alone.

4.2.6 UAV-LiDAR and topographic products at MFC2

The repository includes a high-resolution Digital Terrain Model (DTM) derived from UAV-LiDAR observations acquired over the MFC2 experimental catchment using a DJI Matrice 350 equipped with a Zenmuse L1 sensor. The processed DTM is distributed as a GeoTIFF raster with 1-m spatial resolution together with the associated metadata describing the acquisition and processing workflow. The LiDAR products support terrain analysis, hydrological modelling, drainage-network extraction, microtopographic characterization and integration with hydrogeophysical and remote-sensing observations.

An aerial survey of the MFC2 study site was conducted using a DJI Matrice 350 (M350) drone equipped with a Zenmuse L1 sensor (see Fig. 5B). The system combines a Livox LiDAR sensor, a high-precision inertial measurement unit (IMU), and a stabilized gimbal to acquire high-density three-dimensional point clouds with direct georeferencing supported by the M350 real-time kinematic (RTK) navigation system. To enhance accuracy and reduce the latency in the GNSS (Global Navigation Satellite System) correction data stream, an Emlid RS2+ GPS unit was placed on a fixed tripod placed in the field (see Fig. 5A), thereby acting as a temporary local GNSS base during the survey.

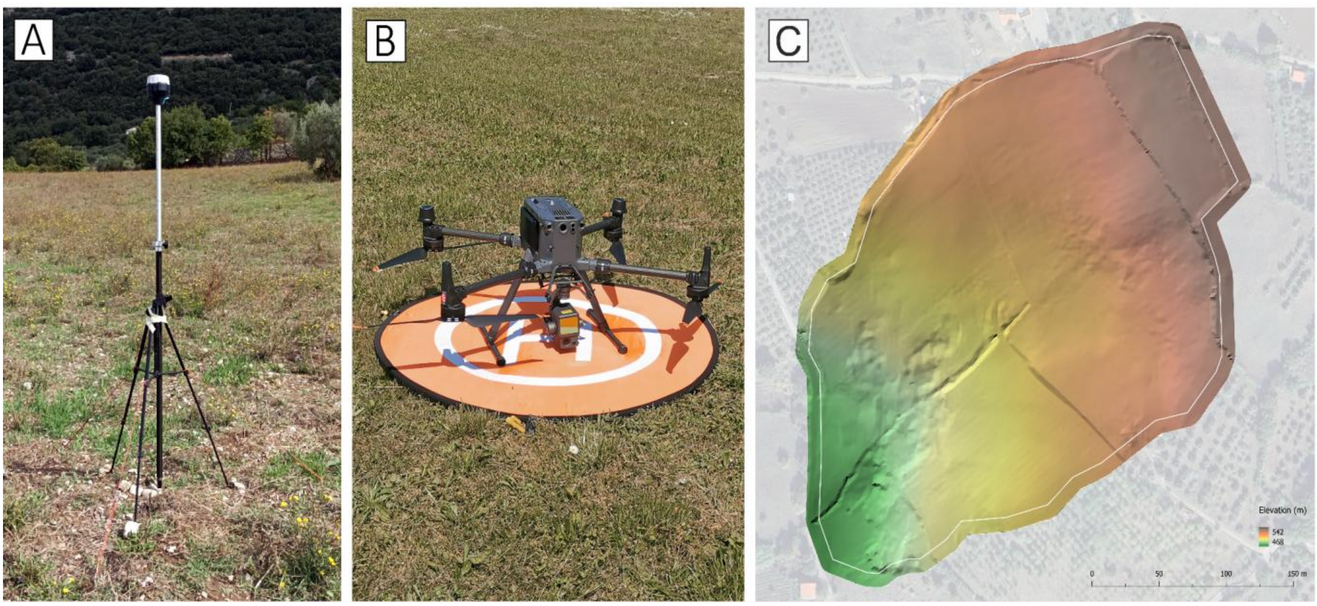

Figure 5: Used tools for aerial survey (A – Emlid Reach RS2+ GPS unit, B – DJI M350 with a Zenmuse L1 lidar onboard) and the resulting digital terrain model of MFC2 site (C).

https://doi.org/10.5194/essd-2026-725
Preprint. Discussion started: 18 September 2026

Prior to the survey, the base station coordinates were established by connecting the receiver to the Campania GNSS network and averaging a fixed RTK solution over a 3 min observation period. The survey was performed at an altitude of 75 m above ground level in terrain-follow mode to account for the site's topographic variability and tree cover. The maximum flight speed was 6 m s^{-1}, with a 50 % overlap between adjacent flight lines. The Zenmuse L1 sensor was configured in triple-return mode with a pulse repetition rate of 160 kHz and repetitive scanning mode. Under these acquisition settings, the expected point cloud density was approximately 330 points m^{-2}, providing a high-resolution representation of the terrain and vegetation structure. The raw data were processed using DJI Terra software (version 5.1.0), resulting in a 3D point cloud of the area, which was then exported into LAS format. The point cloud was subsequently processed in R (R Core Team, 2025) using the lidR package (Roussel et al., 2020). The workflow consisted of identifying last-return points, classifying ground points using the Progressive Morphological Filter algorithm (Zhang et al., 2003), and interpolating the classified ground points to generate a Digital Terrain Model (DTM). The DTM was produced at a spatial resolution of 1 m using the Multilevel B-Spline Approximation (MBA) interpolation algorithm (Lee et al., 1997), as implemented in the MBA package (Finley et al., 2024).

Within the integrated framework, high-resolution topographic information provides the land-surface context necessary to interpret spatial patterns in soil moisture, hydrogeophysical properties, drainage organization, and hydrological connectivity.

4.2.7 Measurement of soil properties and hydraulic characteristics at MFC2

Targeted soil sampling and field measurement campaigns were conducted at MFC2 to characterize the spatial variability of the soil physical and hydraulic properties and to complement the continuous observations provided by the SoilNet monitoring network. Two complementary sampling strategies were adopted: (*i*) sampling at the 20 SoilNet monitoring locations, aimed at providing site-specific soil information associated with the sensor observations, and (*ii*) a regular 25 m sampling grid covering the entire MFC2 experimental catchment, aimed at characterizing soil-property variability at the field scale.

At each of the 20 SoilNet locations, disturbed and undisturbed soil samples were collected from the topsoil. Laboratory analyses were performed to determine particle-size distribution (sand, silt, and clay contents), soil textural class, oven-dry bulk density, soil organic carbon, and saturated hydraulic conductivity. A second, spatially denser sampling campaign was designed using a 25 m regular grid covering the MFC2 catchment. A total of 124 sampling locations were established, at which disturbed and undisturbed topsoil samples were collected. The same suite of physical and hydraulic properties determined at the SoilNet locations was measured on these samples, including particle-size distribution, soil textural class, oven-dry bulk density, and soil organic carbon content. The 124 disturbed samples were also used for laboratory soil spectroscopy.

In each sampling strategy, the disturbed soil samples were air-dried, gently disaggregated, and passed through a 2-mm sieve to determine the following soil attributes:

- Soil particle-size distribution was determined using the sieving technique for the sand-sized particles (effective diameter from 2.0 mm to 0.050 mm) and the hydrometer method for the clay-sized particles (effective diameter less than 0.002 mm) (Gee and Or, 2002; Lazzaro et al., 2023). The textural class of each soil sample was determined according to the United States Department of Agriculture (USDA) classification from the percentages of sand and clay contents;

https://doi.org/10.5194/essd-2026-725
Preprint. Discussion started: 18 September 2026

- Soil organic carbon (SOC) content (%) was measured from the sieved soil sample (fine fraction less than 2.0 mm) using the wet combustion method suggested by Mebius (1960);
- Spectral measurements were performed in the laboratory following the IEEE P4005 protocol (Ben Dor et al., 2024). An Analytical Spectral Devices (ASD) FieldSpec® 3 spectrometer (model FSP 350-2500P) was used to measure diffuse reflectance across 2,151 bands in the visible to shortwave-infrared (VNIR-SWIR) range (350–2,500 nm). The spectral resolution (full-width-half-maximum, FWHM) is approximately 3 nm in the VNIR region (350–1,000 nm) and 10 nm in the SWIR region (1,001–2,500 nm).

Each intact soil core was taken from the topsoil by vertically inserting a steel cylinder, with a volume of 697.1 cm^3 (12.0 cm in height and 8.6 cm in inner diameter). An inverse modeling approach based on the evaporation test of Romano and Santini (1999) was used to determine the soil-water retention (WRF) and hydraulic conductivity (HCF) functions, described through the bimodal relationships developed by Romano et al. (2011; referred to as the bROM model). The bimodal soil-water retention function (bROM-WRF) has the following analytical expression:

$$S_e(h) = w\left\{\frac{1}{2}erfc\left[\frac{\ln\ln(h/h_1)}{\sigma_1\sqrt{2}}\right]\right\} + (1-w)\left\{\frac{1}{2}erfc\left[\frac{\ln\ln(h/h_{m2})}{\sigma_2\sqrt{2}}\right]\right\} \quad (6),$$

where $S_e = (\theta - \theta_r)/(\theta_s - \theta_r)$ is the effective saturation. In this study, the residual soil-water content, θ_r, was set equal to zero, and therefore $S_e = \theta/\theta_s$. In Eq.(6), the symbols h_{m1}, $h_{m2,}$ and σ_1, σ_2 are the scale and shape parameters of the two water retention components, respectively, whereas w is the weighting factor ($0 \leq w \leq 1$) to which a physical meaning can also be given. For details about the development of the closed-form, bimodal hydraulic conductivity function and its analytical expression (bROM-HCF), readers are referred to the paper by Romano et al. (2011).

For the application of hydrological modeling tools, the knowledge of soil-water retention characteristics should be supplemented by information about local values of soil hydraulic conductivity. At each of the 20 SoilNet sensing locations distributed along the two hillsides of the creek, measurements of near-saturated soil hydraulic conductivity ($K_{n\text{-}s}$) were carried out using a mini-disk infiltrometer (MDI; METER Group, Inc., Pullman, WA, USA). The MDI device induces an in-situ infiltration process in a relatively straightforward and expeditious manner; it had a disk diameter of 4.5 cm and was operated by imposing a suction pressure head of 2.0 cm, with the volume of the infiltrated water recorded every 30 s for at least 5 minutes. More details about the MDI device and its operations can be found in the factory user's manual and the paper by Nimmo and Voss (2023). The scatter plot of Fig. 6 indicates a strong correspondence (or statistical association) between the individual values of $K_{n\text{-}s}$ and the corresponding values of soil hydraulic conductivity at h=0 (K_0) of the bROM-HCF model, obtained from laboratory tests on undisturbed soil cores collected in the same positions where the MDI infiltration tests were performed. The Pearson coefficient of determination ($R^2 = 0.986$) quantitatively corroborates this high correspondence.

From an open-air laboratory (OAL) perspective, this scatter plot demonstrates the MDI device's ability to map soil hydraulic conductivity accurately across large areas. Francos et al. (2021) leveraged this method in the MFC2 catchment, pairing MDI infiltration rates with SoilPRO field spectroscopy (Ben Dor et al., 2023) and synchronized Cubert drone overpasses to capture

https://doi.org/10.5194/essd-2026-725
Preprint. Discussion started: 18 September 2026

reliable ground-truth data. However, just as laboratory findings often raise new questions, our fieldwork in the Alento catchment highlights the need for further research, specifically using geophysical surveys and isotopic measurements to analyze soil-vegetation interactions.

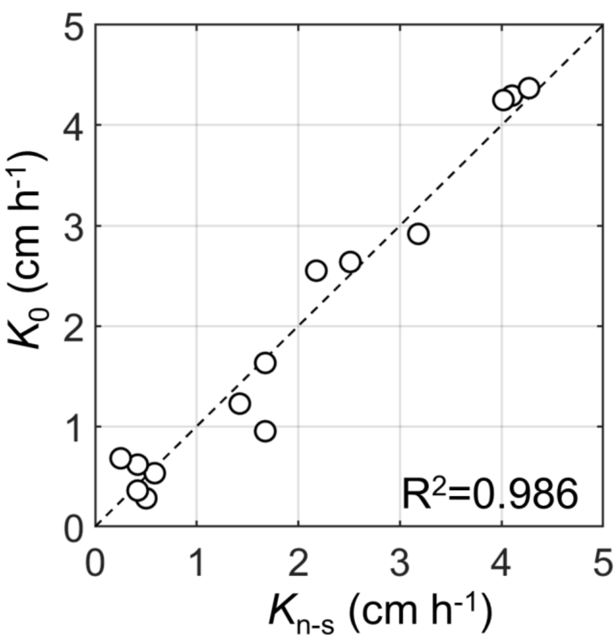

Figure 6: Comparison of near-saturated soil hydraulic conductivity (K_{n-s}) values, measured in MFC2 with the mini-disk infiltrometer, and soil hydraulic conductivity at h=0 (K_0) values of the bROM-HCF model (Romano et al., 2011). The black dashed line is the 1:1 line. The value of the coefficient of determination (R^2) is reported in the plot.

It is worth noting that measurements conducted at the SoilNet locations directly link the soil physical and hydraulic characteristics to the continuous sensor observations, whereas the 25-m grid provides a substantially denser representation of their spatial variability across MFC2. This nested sampling design integrates point-scale observations with field-scale spatial variability and supports soil-property mapping, investigation of spatial controls on soil-water dynamics, development and evaluation of pedotransfer and spectral transfer functions, and parameterization and evaluation of process-based hydrological models (Nasta et al., 2026).

Finally, the soil physical properties, spectral reflectance measurements, observed saturated hydraulic conductivity, and field-derived near-saturated hydraulic conductivity values described above are provided in the repository. However, the underlying experimental soil-water retention and hydraulic conductivity data obtained from the laboratory evaporation experiments are not included in the publicly available dataset.

5. Potential applications of the ARC dataset

The ARC is designed both as a long-term environmental repository and as a research infrastructure supporting hypothesis-driven investigations of Mediterranean Critical Zone processes. By integrating hydrometeorological, hydrological, pedological, hydrogeophysical, and land-use data across multiple spatial and temporal scales, the dataset enables a wide range of scientific applications. Below, two distinct cases illustrate its potential use by the scientific community: (*i*) characterizing the influence of Mediterranean climate seasonality on Critical Zone functioning, and (*ii*) quantifying long-term impacts of land-use and land-cover change on agroecosystem functions and services. A notable strength of the ARC dataset is the partial temporal and spatial overlap among observations obtained using independent techniques. This overlap provides opportunities for cross-technique consistency assessment across observation scales. For instance, CRNS-based field-scale soil-water content can be compared with distributed SoilNet measurements and campaign-based TDR observations, while EMI and ERT surveys provide complementary information on the spatial organization of subsurface electrical properties. Stable water isotopes provide an independent process-based constraint on water sources and flow pathways. These comparisons allow users to distinguish differences attributable to measurement uncertainty from those arising from differences in spatial support, temporal resolution, measurement depth, and process sensitivity.

These examples are intended to illustrate the extensive applicability of the Alento dataset for environmental monitoring, process understanding, model development, and climate-change impact assessments in Mediterranean and comparable environments, rather than providing exhaustive process-based analyses.

5.1. Characterizing Mediterranean climate seasonality and Critical Zone functioning

According to the IPCC (2022), the Mediterranean region is expected to experience progressively warmer conditions, greater hydroclimatic variability, and an increasing frequency of extreme events during the twenty-first century. Although projected changes in annual precipitation totals remain uncertain, precipitation will likely concentrate into fewer, high-intensity events separated by severe droughts, increasing water stress in agricultural landscapes (Nasta et al., 2013).

Monitoring at the MFC1 experimental site between 2006 and 2009 provides an integrated baseline describing the hydrological functioning of a Mediterranean agricultural landscape characterized by mixed cropland, shrubs, and scattered trees (Fig. 7). Specifically, Fig. 7a illustrates the seasonal decoupling of daily precipitation (P) and reference potential evapotranspiration (ET_0): rainfall is concentrated from late fall to early spring, whereas ET_0 peaks during hot summer. Streamflow (Q) at the sub-catchment outlet exhibits the typical torrential regime of many Mediterranean creeks, where discharge peaks synchronize with rainfall, followed by minimal summer flow. Spatial-average near-surface soil moisture (θ, 0-15 cm) reflects rapid wetting-drying cycles, while piezometer water levels (WL), referenced to the catchment outlet elevation (24 m for W280, 7 m for W342, 3 m for W345, and 16 m for W324), track seasonal groundwater fluctuations relative to the stream base.

https://doi.org/10.5194/essd-2026-725
Preprint. Discussion started: 18 September 2026

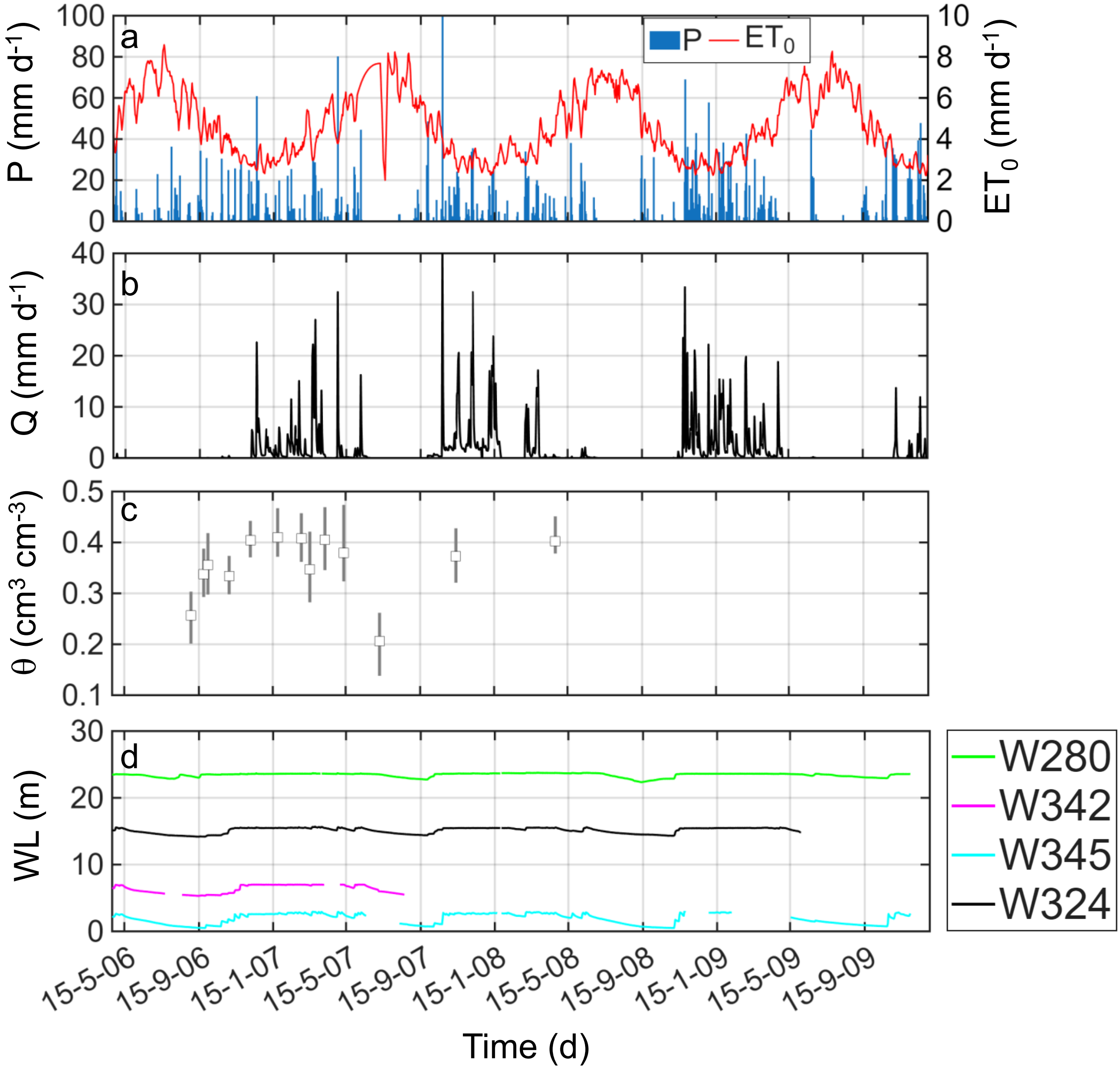

645 **Figure 7: Time series of environmental variables recorded at the MFC1 sub-catchment from 2006 up to 2009: a) Rainfall (*P* in mm d^{-1}; blue bars) and reference potential evapotranspiration (*ET_0* in mm d^{-1}; red curves); b) streamflow (Q in mm d^{-1}) recorded at the outlet; c) spatial-average (white squares) soil moisture, θ (in cm^3 cm^{-3}), and its 25th and 75th percentiles (gray bars), d) groundwater levels (WL) recorded at wells W280, W342, W345, and W324 and expressed relative to the elevation of the MFC1 catchment outlet. The corresponding elevation differences between the well locations and the outlet are 24, 7, 3, and 16 m, respectively.**

https://doi.org/10.5194/essd-2026-725
Preprint. Discussion started: 18 September 2026

For the dominantly forested site of GOR1, Figure 8 further highlights this seasonal decoupling. Continuous point-scale (GS3 sensors) and field-scale (Cosmic-Ray Neutron Sensor, CRNS) soil moisture observations demonstrate the value of multi-scale monitoring for capturing deep-soil water dynamics under strong evaporative demand (Nasta et al., 2024).

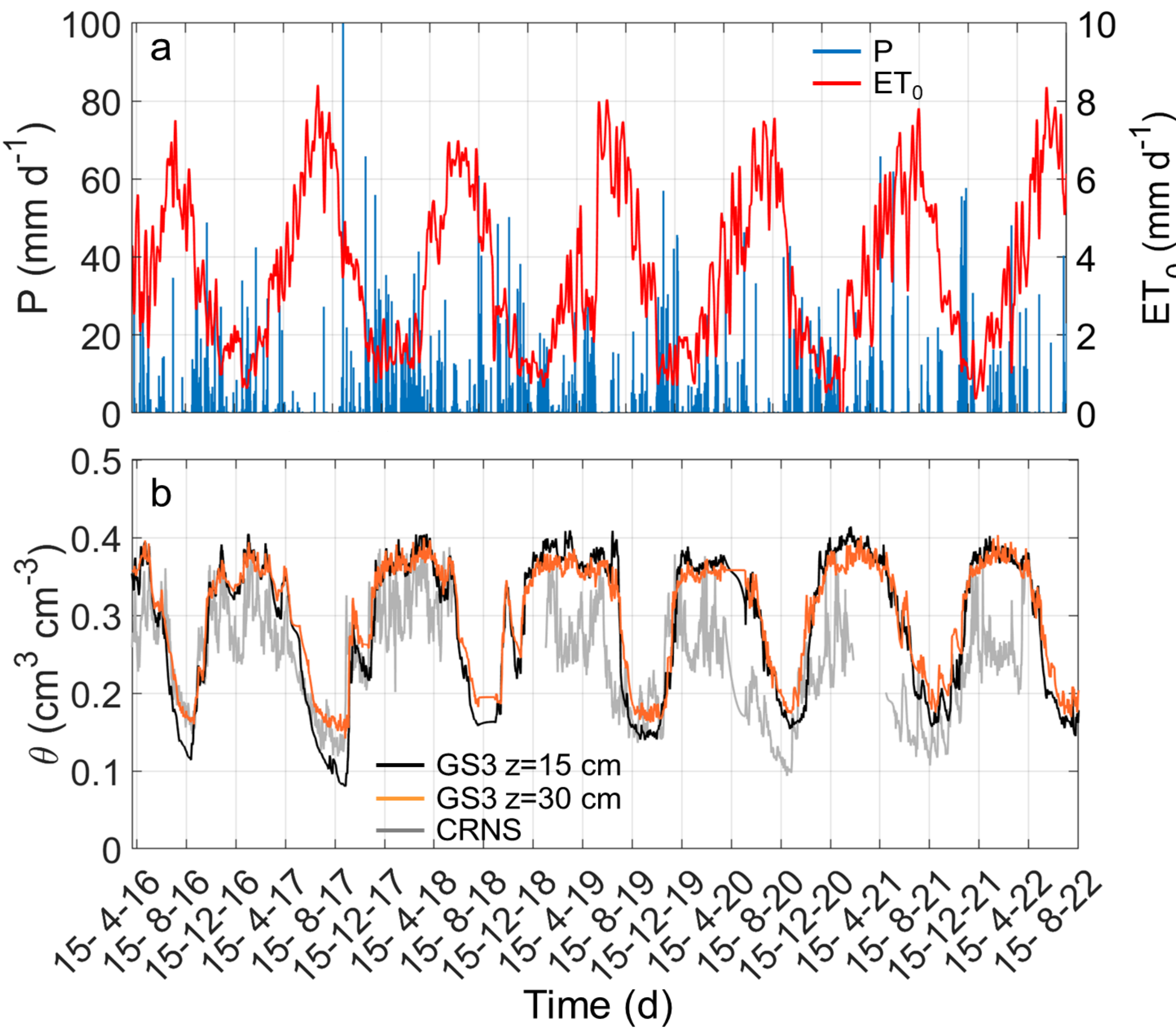

Figure 8: Time series of environmental variables recorded at the GOR1 sub-catchment from mid-2016 up to mid-2022. Plot 7a (top) shows rainfall (*P* in mm d^{-1}; blue bars) and reference potential evapotranspiration (ET_0 in mm d^{-1}; red curves). Plot 7b (bottom) shows soil moisture, θ (in cm^3 cm^{-3}), as measured by the GS3 sensors at point-scale (black and orange curves). The gray curve depicts field-scale soil moisture as observed by the CRNS.

Research activities at MFC2 exemplify the strength of coupling a CZO with an Open-Air Laboratory by integrating continuous monitoring with detailed soil hydraulic characterization to evaluate rainfall partitioning across opposing hillsides in flysch geology. This objective is particularly relevant because (*i*) the V-shaped terrain configuration of the MFC2 permits direct comparison of the hydrological behavior of the opposing hillsides of the creek, and (*ii*) runoff generation mechanisms remain insufficiently understood in Mediterranean catchments developed on flysch geological formations.

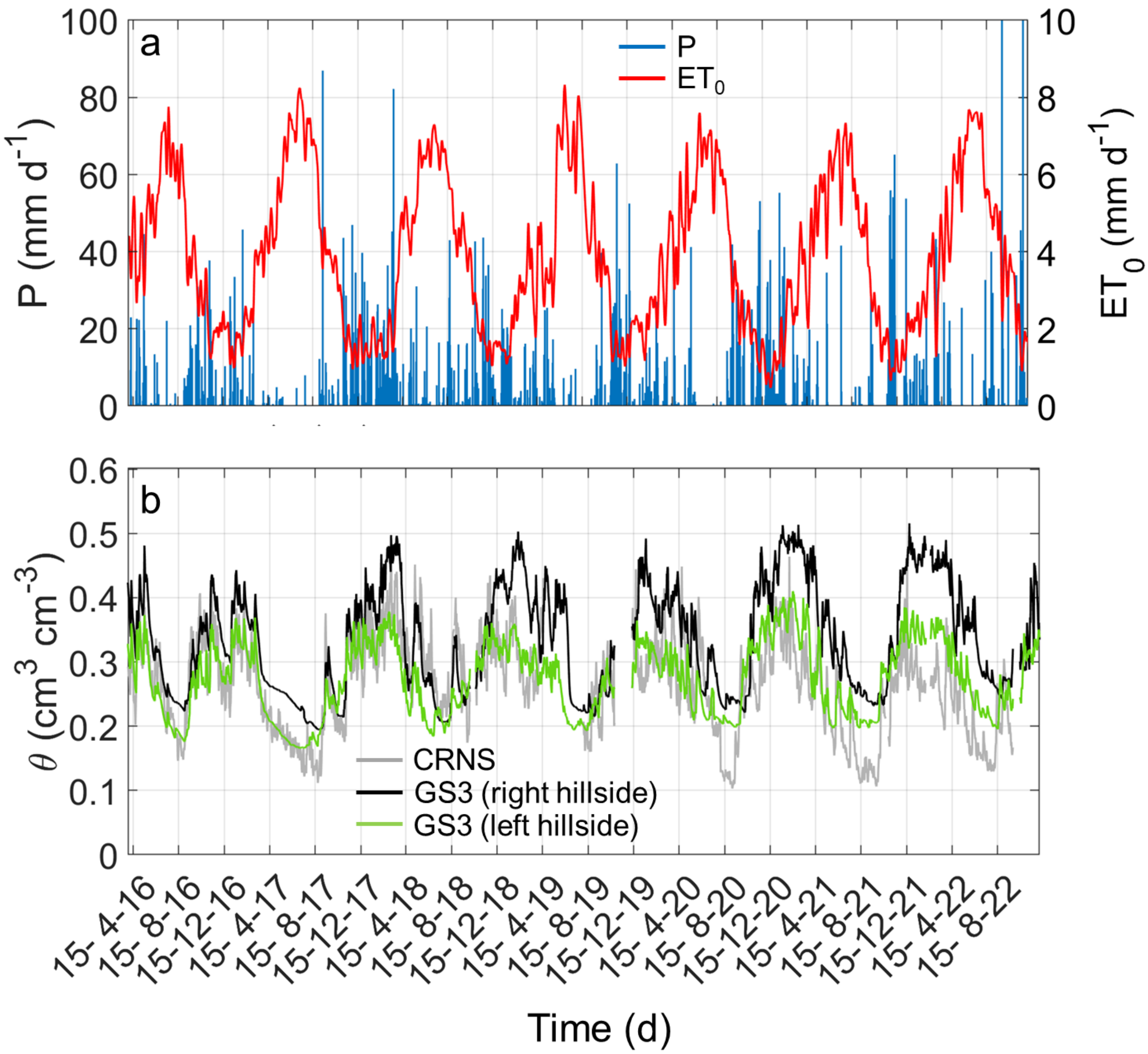

Figure 9: Time series of environmental variables recorded at the MFC2 sub-catchment from mid-2016 up to mid-2022: a) rainfall (*P* in mm d^{-1}; blue bars) and reference potential evapotranspiration (*ET*$_0$ in mm d^{-1}; red lines), and b) soil moisture, θ (in cm^3 cm^{-3}) measured by the GS3 sensors at the point scale. The black and green lines represent the spatial average of the ten GS3 sensors installed at the soil depth of 15 cm on the right and left hillsides, respectively. The gray line represents the field-scale soil moisture obtained by the CRNS.

https://doi.org/10.5194/essd-2026-725
Preprint. Discussion started: 18 September 2026

MFC2 provides a valuable natural laboratory for investigating the combined effects of climatic seasonality and soil spatial heterogeneity on soil moisture dynamics (see Fig. 9). Although precipitation (P) and ET_0 determine the overall seasonal evolution of soil moisture (Fig. 9a), θ values measured at 15 cm depth reveal persistent differences between the two opposing hillsides (Fig. 9b). The green line (representing the average of ten sensors on the left hillside) consistently shows different soil moisture values than the black line (representing the average of ten sensors on the right hillside). This divergence is largely due to the higher clay content found on the right hillside, which increases its soil-water storage capacity relative to the left hillside. Although the average soil moisture on both hillsides follows general wetting and drying cycles, there are differences between the point-scale sensor averages and the field-scale soil moisture recorded by the Cosmic-Ray Neutron Sensor (CRNS) (gray line in Fig. 9b). The heterogeneity in soil moisture at the hillslope scale emphasizes the fact that the V-shaped terrain configuration of MFC2, with variations in soil textural properties, should affect the hydrological response of this sub-catchment.

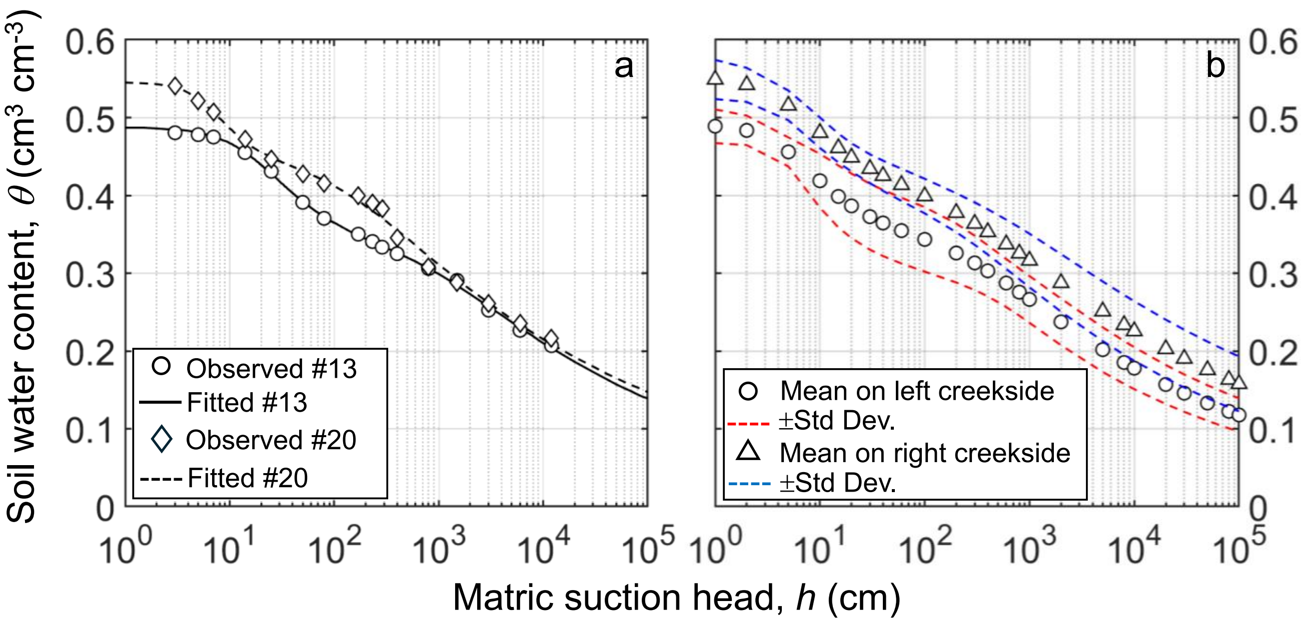

Figure 10: Soil-water retention functions [$\theta(h)$; WRF] obtained from undisturbed soil cores collected at the MFC2 sub-catchment: a) observed $\theta(h)$ data points for soil core #13 and soil core #20 fitted by the bimodal soil-water retention model bROM-WRF; b) mean water retention data points, and relevant confidence intervals, for the left and right creekside.

The observed differences in hillslope soil moisture dynamics are fundamentally rooted in distinct soil physical and hydraulic properties of the two hillsides, as detailed in Section 4.2.7. The soil physical data reveal that the two hillsides of the creek in MFC2 behave quite similarly in terms of oven-dry bulk density and soil organic carbon content, whereas the greatest

https://doi.org/10.5194/essd-2026-725
Preprint. Discussion started: 18 September 2026

differences are evident in terms of soil texture. Specifically, soils lying on the left hillside have, on average, lower sand content and greater silt content than the soils on the right hillside. Both creek hillsides, on the other hand, are characterized by relatively high percentages of clay content, ranging from a minimum value of 23.47% on the left side to a maximum of 48.67% on the right side. On average, the right hillside of the creek contains greater fractions of clay particles. The contrasting soil hydraulic behavior of the two hillsides of the creek is further illustrated by their soil-water retention functions (WRFs) of Fig. 10. Figure 10a compares representative WRFs for soil cores #13 (located on the left hillside of the creek) and #20 (located on the right hillside of the creek), whereas Fig. 10b presents the mean values of all water retention data points measured along either the right or left creek hillsides, together with the colored dashed curves representing the plus/minus one standard deviation bands (i.e., ±1 Std.Dev.).

Complementary electromagnetic induction (EMI) surveys map these seasonal dynamics in space (Fig. 11). Under wet conditions (Dec 2020, 341.6 mm rainfall; Fig. 11a), low electrical resistivity dominates, whereas dry conditions (Aug 2021, 6.3 mm rainfall; Fig. 11b) markedly increase resistivity. The highest conductivity zones align with low-lying, clay-rich areas.

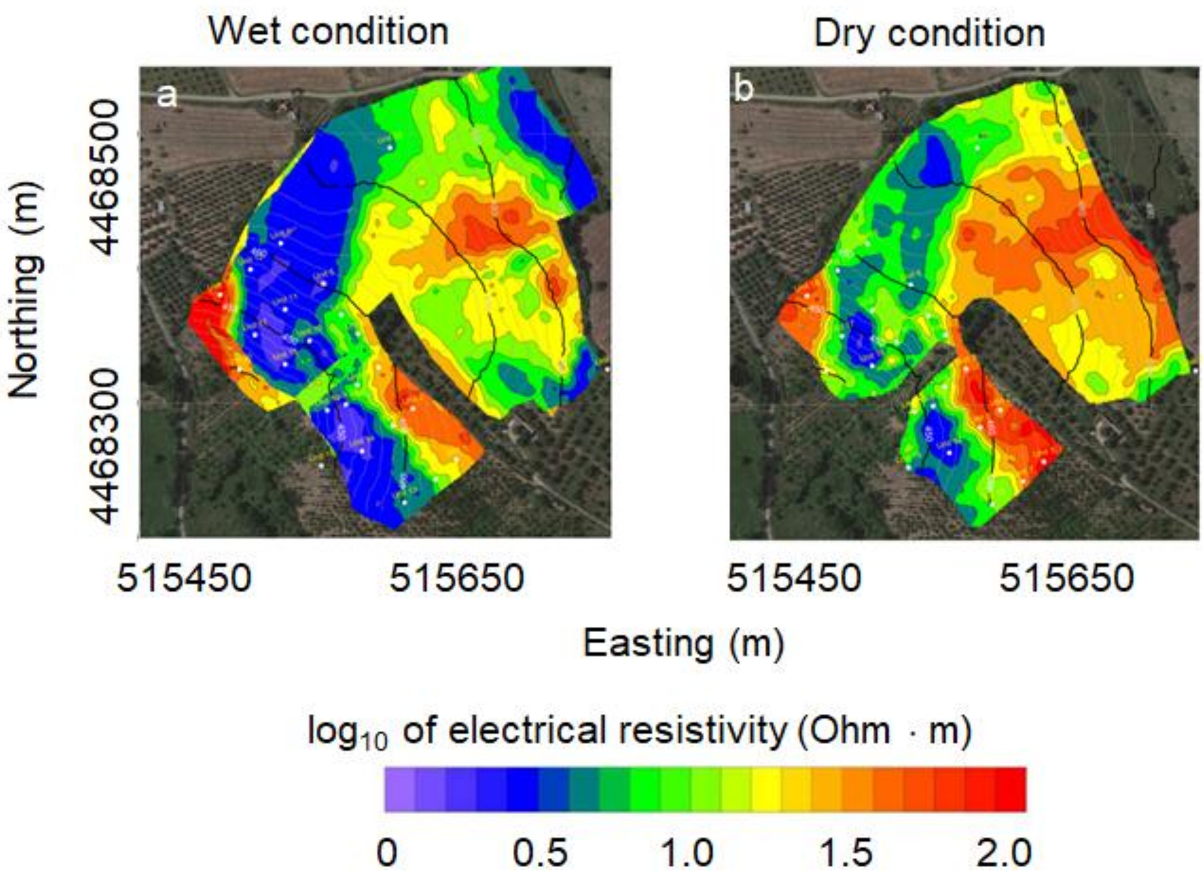

Figure 11: EMI-derived maps of $\log_{10}$-values of electrical resistivity at 0.50 m depth in MFC2 on a) 15th December 2020 (wet condition) and b) 5th August 2021 (dry condition).

https://doi.org/10.5194/essd-2026-725
Preprint. Discussion started: 18 September 2026

By pairing long-term atmospheric and soil-vegetation monitoring with targeted hydrogeophysical and soil physical and hydraulic measurements, the UARC provides a transferable framework for evaluating how Mediterranean catchments store, redistribute, and release water under intensifying climatic stress.

5.2. Assessing land-use and land-cover change impacts on agro-ecosystem functions and services

Post World War II rural depopulation has driven major LULC shifts in the UARC and changes in the traditional agro-pastoral activities. Historical land-use maps, based on ground surveys in 1955, 1998, and 2015, show a retreat of arable lands and pastures (from approximately 70% combined in 1955 to less than 10% in 2015; see Fig. 12) and a concurrent expansion of forest cover, which now dominates nearly 70% of the upper catchment. Readers interested in evaluating these changes are directed to the paper by Nasta et al. (2017). This shift, in conjunction with inadequate forest maintenance, heightens the risk of wildfire during periods of drought, which is a common occurrence in many hilly and mountainous areas of the Mediterranean region. The long-term LULC record provides a landscape-scale boundary condition for interpreting changes in vegetation, soil-water dynamics, evapotranspiration, groundwater recharge, and catchment water yield.

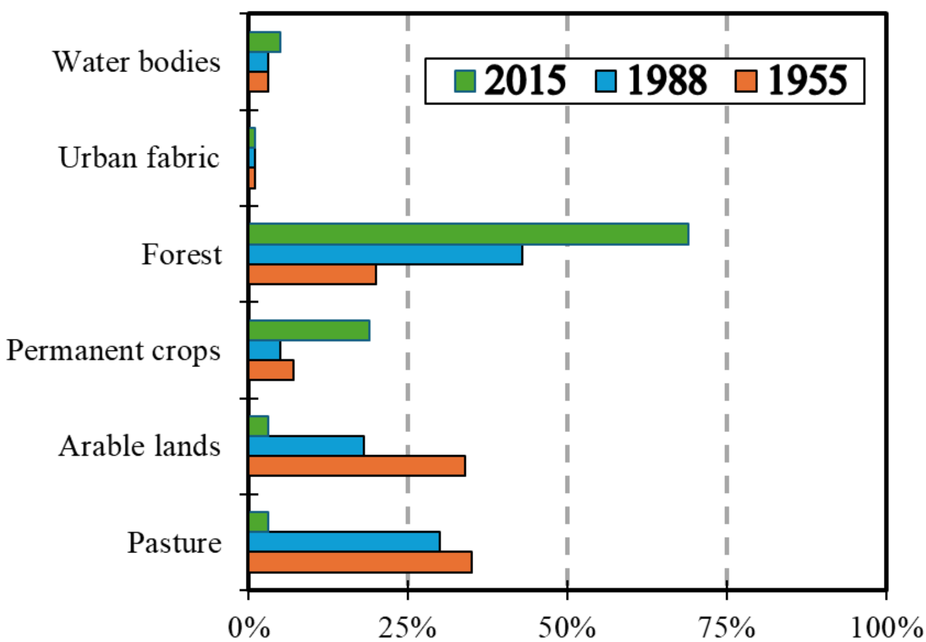

Figure 12: Evolution of land use percentages in the Upper Alento River Catchment (UARC) for the years 1955, 1998, and 2015. The dataset for the period 1988-2015 has been refined using satellite imagery, highlighting the transition from agricultural dominance to widespread afforestation following rural abandonment.

https://doi.org/10.5194/essd-2026-725
Preprint. Discussion started: 18 September 2026

Open Access Earth System Science Data Discussions

The weather station, located near the town of Gioi Cilento, was deployed in 1920 and has the longest time series (about 100 years) of observational data in the Alento River catchment. Figure 13 compares annual precipitation (P), recorded at the Gioi Cilento rain gauge, and annual water yield (WY), measured at the Piano della Rocca dam over the study period (1995-2020).

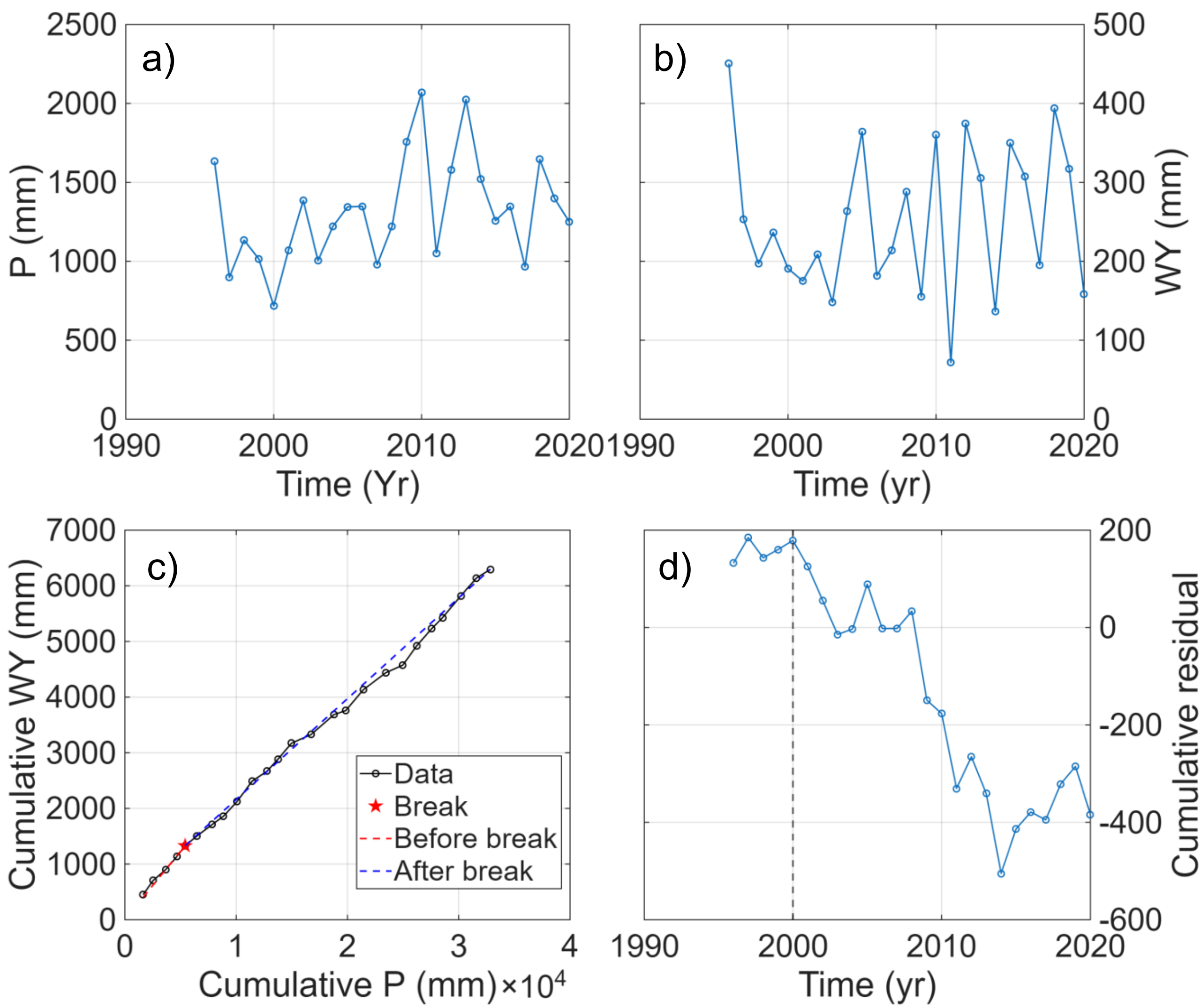

Figure 13. a) annual precipitation (P) recorded at the Gioi rain gauge, b) annual water yield (WY) measured at the dam, c) double-mass curve relating cumulative precipitation to cumulative water yield (black dots and line indicate the observed data while the colored dashed lines depict the fitted data before and after the breakpoint identified in the year 2000), and d) cumulative residuals of the WY–P relationship (the vertical dashed line depicts the breakpoint in 2000).

While annual P (Fig. 13a) and WY (Fig. 13b) series show substantial interannual variability without evident monotonic trends (Pettitt test $p = 0.10$ and $p = 1.00$, respectively), the double-mass curve in Fig. 13c reveals a structural breakpoint in the year

https://doi.org/10.5194/essd-2026-725
Preprint. Discussion started: 18 September 2026

2000. Before 2000, the cumulative WY–P slope was approximately 0.25, dropping to about 0.18 afterward, a 26.4% decrease in the water-yield-to-precipitation ratio. This shift is consistent with increased evapotranspiration and subsurface water retention associated with the documented expansion of forest cover, although other climatic, hydrological, and land-management changes may also have contributed to the observed response.

In practical terms, the change in the cumulative WY–P relationship indicates that a smaller fraction of annual precipitation was converted into catchment water yield after approximately 2000. The temporal correspondence with the documented expansion of forest cover (see Fig. 12) suggests that changes in vegetation and associated evapotranspiration and subsurface water storage may have contributed to this shift. This apparent shift should be interpreted with caution, since the Pettitt test did not detect a statistically significant change point in the annual series, consistent with a gradual rather than abrupt catchment response. Therefore, because other climatic, hydrological, and land-management factors may also have changed over the same period, the observed relationship should be interpreted as an association rather than as evidence of a direct causal effect of forest expansion. One of the main challenges in hydrology is establishing causal relationships between landscape change and catchment response because suitable long-term datasets are rarely available. The Alento datasets overcome this limitation by documenting a profound and well-quantified transformation from an agro-pastoral landscape to a predominantly forested one over a period of approximately sixty years.

6. Data availability

The complete dataset supporting the findings of this study is openly available via the Figshare repository at https://doi.org/10.6084/m9.figshare.31229608 (Romano et al., 2026). The repository is organized into five primary folders reflecting the spatial and thematic components of the Alento observatory.

7. Conclusions

7.1. Broader scientific relevance and transferability

The ARC dataset extends beyond a conventional catchment hydrological monitoring dataset by providing coordinated observations across multiple Critical Zone components and by linking them through complementary measurements of water, energy, and solute dynamics. Atmospheric observations characterize environmental forcing; soil and hydrogeophysical measurements constrain water storage and subsurface heterogeneity; stable water isotopes provide information on water sources and pathways; vegetation and land-surface observations characterize vegetation–water interactions and spatial variability; and groundwater and surface-water observations integrate these processes at the catchment scale. The resulting framework provides an observational basis for investigating interactions among Critical Zone components rather than treating individual data streams independently.

https://doi.org/10.5194/essd-2026-725
Preprint. Discussion started: 18 September 2026

Although the observations are geographically concentrated within the Alento River Catchment, the scientific questions addressed by the dataset are broadly transferable. These include the dependence of hydrological processes on observation scale, the role of soil and subsurface heterogeneity in water storage and redistribution, water-source partitioning and hydrological connectivity, vegetation–water interactions, and the use of multiple observations to evaluate process-based environmental models. The dataset therefore provides a well-documented experimental system for testing scaling approaches, conducting model intercomparisons, evaluating Earth Observation products, and comparing observations with those from other Critical Zone observatories and environmental research infrastructures. Its broader relevance derives from the transferability of these scientific questions and methodological challenges rather than from statistical representativeness of the Alento Catchment.

7.2. Final remarks

A distinguishing feature of the ARC is its dual role as both a long-term Critical Zone observatory and an Open-Air Laboratory. Continuous monitoring provides the temporal context necessary to characterize environmental variability and change, whereas targeted field campaigns provide spatially distributed and process-specific observations necessary to interpret those changes. The deliberate overlap of these layers enables the examination of long-term environmental dynamics in conjunction with process-level observations across nested spatial and temporal scales. This transformation of the dataset from a collection of individual measurements into an integrated Critical Zone resource is a key feature of the approach.

The primary novelty of the ARC dataset, therefore, does not lie in any singular measurement technique, but rather in the coordinated integration of complementary observations across multiple Critical Zone components and spatial and temporal scales. Continued monitoring and future field campaigns will expand the dataset while preserving data provenance and version history, further increasing its value as a long-term observational resource for Mediterranean Critical Zone and Earth system research. The resulting combination of complementary observations also provides an empirical basis for evaluating observation-scale effects, assessing cross-technique consistency, and constraining process-based models across nested spatial and temporal scales.

https://doi.org/10.5194/essd-2026-725
Preprint. Discussion started: 18 September 2026

APPENDIX

A1. Data repositories and access

The ARC repository has been designed as an integrated observation framework, rather than as a collection of independent datasets. In this framework, complementary measurements acquired at different spatial and temporal scales can be analyzed collectively. Standardized metadata, common temporal conventions, harmonized measurement protocols, and open data access facilitate interdisciplinary applications and maximize long-term data reuse.

The ARC dataset described in this paper is openly available through the Figshare repository (Romano et al., 2026; https://doi.org/10.6084/m9.figshare.31229608). The repository has been organized to facilitate data discovery, interoperability, and reuse by the hydrological, Critical Zone, and Earth System science communities. The dataset combines long-term environmental monitoring with complementary field observations collected at multiple spatial scales, ranging from individual soil profiles to the entire river catchment. This dataset is provided under a Creative Commons Attribution 4.0 International License (CC BY 4.0). Future releases will receive version updates while preserving previous releases.

A2. File organization, metadata structure, and data formats

To simplify data access, the repository is organized into five thematic folders corresponding to the main monitoring sites and data products (Table A1):

1. **LARC** – Lower Alento River Catchment observations;
2. **MFC1** – hillslope monitoring dataset;
3. **MFC2** – agricultural Critical Zone observatory;
4. **GOR1** – forested Critical Zone observatory;
5. **DEM_1m_MFC2** – high-resolution UAV-LiDAR digital terrain model.

Because some missing observations resulted from field accessibility, seasonal vegetation conditions, instrument limitations, or targeted sampling strategies, missingness should not necessarily be assumed to be random.

https://doi.org/10.5194/essd-2026-725
Preprint. Discussion started: 18 September 2026

Open Access Earth System Science Data Discussions

Table A1. Repository folder, file name, data type, units and record details of the shared dataset.

Repository folder	File	Data Type	Units	Record	Frequency	Time aggregation	Missing
LARC	DAM_P_ET0.csv	P, ET_0	mm d^{-1}	1994–2021	Daily	-	0.076 %
	DAM_WL_WY.csv	WL, WY	m, mm d^{-1}	1994–2021	Daily	-	0%
	LARC_OUTLET.csv	H	m	2003–2022	Daily	-	8.9%
MFC1	MFC1_P_ET0.csv	P, ET_0	mm d^{-1}	2006–2009	Hour	Daily	0%
	MFC1_Q_DtGW.csv	Q, WL	mm d^{-1}, m	2006–2009	10-min	Daily	20.6%
	MFC1_TDR_SM.xlsx	θ	$cm^3\ cm^{-3}$	2006-2008	Snapshots	-	33.9%
MFC2	MFC2_P_ET0.csv	P, ET_0	mm d^{-1}, mm d^{-1}	2016-2023	Hour	Daily	1.3%
	MFC2_SM_CRNS.csv	CRNS-based θ	$cm^3\ cm^{-3}$	2016-2023	15-min	Daily	16.4%
	MFC2_SM_z15cm.csv	θ at depth of 15 cm	$cm^3\ cm^{-3}$	2016-2023	15-min	Daily	4.9%
	MFC2_SM_z30cm.csv	θ at depth of 30 cm	$cm^3\ cm^{-3}$	2016-2023	15-min	Daily	4.9%
	MFC2_POT_z15cm.csv	h at depth of 15 cm	kPa	2016-2023	15-min	Daily	4.9%
	MFC2_GRID_124_SOIL_PROPERTIES.csv	soil properties		2016-2023	Snapshots	-	0%
	MFC2_GRID_124_SPECTRA.csv	spectral measurements		2016-2023	Snapshots	-	0%
	MFC2_SOILNET_20_SOIL_PROPERTIES.csv	soil properties		2016-2023	Snapshots	-	0%
	MFC2_POT_z30cm.csv	h at depth of 30 cm	kPa	2016-2023	15-min	Daily	12.9%
	MFC2_ISOTOPES.xlsx	δ^2H, $\delta^{18}O$	‰	2020-2022	Snapshots	-	16.5%
	MFC2_TDR_SM.xlsx	θ	$cm^3\ cm^{-3}$	2018-2021	Snapshots	-	0%
	csv files in MFC2_EMI folder	EMI response	ppm	2020-2021	Snapshots	-	0%
	csv files in MFC2_ERT folder	Electrical resistivity	Ω m	2020-2021	Snapshots	-	0%
DEM_1m_MFC2	MFC2_LiDAR_DEM.tif	Elevation	m	1-m resolution via UAV-LiDAR survey		-	0%
GOR1	GOR1_P_ET0.csv	P, ET_0	mm d^{-1}, mm d^{-1}	2016-2023	Hour	Daily	2.4%
	GOR1_SM_CRNS.csv	CRNS-based θ	$cm^3\ cm^{-3}$	2016-2023	15-min	Daily	22.32 %
	GOR1_SM_z15cm.csv	θ at depth of 15 cm	$cm^3\ cm^{-3}$	2016-2023	15-min	Daily	4.9%
	GOR1_SM_z30cm.csv	θ at depth of 30 cm	$cm^3\ cm^{-3}$	2016-2023	15-min	Daily	4.9%
	GOR1_POT_z15cm.csv	h at depth of 15 cm	kPa	2016-2023	15-min	Daily	4.9%
	GOR1_POT_z30cm.csv	h at depth of 30 cm	kPa	2016-2023	15-min	Daily	12.9%
	GOR1_ISOTOPES.xlsx	δ^2H, $\delta^{18}O$	‰	2020-2022	Snapshots	-	33.75 %
	GOR1_TDR_SM.xlsx	θ	$cm^3\ cm^{-3}$	2018-2021	Snapshots	-	0%
	csv files in GOR1_EMI folder	EMI response	ppm	2020-2021	Snapshots	-	0%

https://doi.org/10.5194/essd-2026-725
Preprint. Discussion started: 18 September 2026

csv files in GOR1_ERT folder	Electrical resistivity	Ω m	2020-2021	Snapshots	-	0%

Each folder contains fully documented datasets together with standardized variable names, units, temporal resolution, and metadata describing the monitoring period and measurement protocols. The datasets include continuous observations collected automatically by monitoring stations as well as data obtained during dedicated field campaigns.

The repository integrates observations covering the principal components of the Critical Zone water cycle, including meteorological forcing, soil moisture, soil matric potential, groundwater levels, streamflow, reservoir inflows, water yield, soil hydraulic properties, stable water isotopes, and high-resolution topographic information. Collectively, these observations provide a comprehensive description of water storage and fluxes across the atmosphere–vegetation–soil–groundwater continuum.

The modular organization of the repository is a feature that ensures that future releases can incorporate additional observations while maintaining compatibility with previous versions. This strategy fosters long-term reproducibility and facilitates the progressive expansion of the Alento integrated multiscale observation framework without compromising data continuity.

All files adopt a standardized Year–Month–Day timestamp convention, SI units where applicable, and standard missing-value flags ("Nan"). No gap-filling or interpolation procedures were applied, ensuring that the published datasets faithfully reproduce the validated field observations.

A2.1 LARC folder

The LARC folder contains three comma-separated value (CSV) files describing the long-term hydrological observations collected in the Lower Alento River Catchment (LARC).

DAM_P_ET0.csv contains the daily observations of P and ET_0 associated with the Piano della Rocca reservoir. The structure and variables included in this file are described in Table A2.1a.

Table A2.1a. Variables, descriptions, and units included in the DAM_P_ET0.csv file

Column	Description	Unit
Year	Calendar year	–
Month	Calendar month	–
Day	Day of month	–
P	Daily precipitation	mm d^{-1}

https://doi.org/10.5194/essd-2026-725
Preprint. Discussion started: 18 September 2026

Column	Description	Unit
ET_0	Daily reference evapotranspiration	mm d^{-1}

DAM_WL_WY.csv contains the daily observations of water level (WL) and water yield (WY) associated with the Piano della Rocca reservoir. The structure and variables included in this file are described in Table A2.1b.

Table A2.1b. Variables, descriptions, and units included in the DAM_WL_WY.csv file

Column	Description	Unit
Year	Calendar year	–
Month	Calendar month	–
Day	Day of month	–
WL	Daily reservoir water level	m
WY	Daily water yield estimated from the reservoir water balance	mm d^{-1}

Daily timestamps follow the Year–Month–Day format. Water yield (WY) represents the catchment inflow normalized by the drainage area of the Upper Alento River Catchment, as described in Sect. 3.2.

LARC_OUTLET.csv contains the daily hydrometric observations collected at the outlet of the Lower Alento River Catchment. The structure and variables included in this file are described in Table A2.1c.

Table A2.1c. Variables, descriptions, and units included in the LARC_OUTLET.csv file

Column	**Description**	**Unit**
Year	Calendar year	–
Month	Calendar month	–
Day	Day of month	–
H	Daily Alento River water level at the LARC outlet	m

The river stage is provided as the measured water level and is intended for hydrological analyses, trend assessment, and comparison with reservoir dynamics.

https://doi.org/10.5194/essd-2026-725
Preprint. Discussion started: 18 September 2026

A2.2 MFC1 folder

The MFC1 folder contains two comma-separated value (CSV) files and one Excel file (XLSX) describing the hillslope-scale monitoring activities carried out at the MFC1 experimental catchment between 2006 and 2009. The datasets include continuous hydrometeorological observations together with campaign-based soil moisture measurements. MFC1_P_ET0.csv contains the daily observations of P and ET_0 associated with the weather station located at MFC1. The structure and variables included in this file are described in Table A2.2a.

Table A2.2a. Variables, descriptions, and units included in the MFC1_P_ET0.csv file

Column	Description	Unit
Year	Calendar year	–
Month	Calendar month	–
Day	Day of month	–
P	Daily precipitation	mm d^{-1}
ET_0	Daily reference evapotranspiration	mm d^{-1}

MFC1_Q_DtGW.csv contains the daily observations of streamflow (Q) and depth to groundwater in four wells (W). The structure and variables included in this file are described in Table A2.2b.

Table A2.2b. Variables, descriptions, and units included in the MFC1_Q_DtGW.csv file

Column	Description	Unit
Year	Calendar year	–
Month	Calendar month	–
Day	Day of month	–
Q	Daily streamflow at the catchment outlet	mm d^{-1}
W280	Depth to groundwater in well W280	m
W324	Depth to groundwater in well W324	m
W342	Depth to groundwater in well W342	m
W345	Depth to groundwater in well W345	m

https://doi.org/10.5194/essd-2026-725
Preprint. Discussion started: 18 September 2026

Groundwater observations represent the depth from the ground surface to the groundwater table measured in the four monitoring wells. Streamflow is expressed as catchment-equivalent water depth (mm d^{-1}).

MFC1_TDR_SM.xlsx contains the campaign-based soil moisture surveys conducted using a portable time-domain reflectometer (TDR). The dataset comprises measurements collected during 13 sampling campaigns conducted between 1 September 2006 and 24 April 2008 at 112 predefined sampling locations. Each row corresponds to a sampling location, identified by its spatial coordinates, whereas the soil moisture observations from the 13 sampling campaigns are organized in separate columns, each identified by the corresponding sampling date. The structure and variables included in the file are described in Table A2.2c.

Table A2.2c. Variables, descriptions, and units included in the MFC1_TDR_SM.xlsx file. Each row represents one of the 112 predefined sampling locations, whereas the date-labelled columns contain volumetric soil water content measured during the 13 sampling campaigns.

Column	Description	Unit
POSITION	Sampling point identifier	–
X	Easting coordinate	m
Y	Northing coordinate	m
2006-09-01 ... 2008-04-24	Volumetric soil water content measured during each field campaign	$cm^3\ cm^{-3}$

A2.3 MFC2 folder

The MFC2 folder contains the most comprehensive dataset of the Alento River Catchment Observatory, integrating continuous hydrometeorological observations with measurements of soil properties. The datasets are organized into separate files according to the monitored variable.

MFC2_P_ET0.csv contains the daily observations of P and ET_0 associated with the weather station located at MFC1 (in proximity to MFC2). The structure and variables included in this file are described in Table A2.3a.

Table A2.3a. Variables, descriptions, and units included in the MFC2_P_ET0.csv file

Column	Description	Unit
Year	Calendar year	–
Month	Calendar month	–

https://doi.org/10.5194/essd-2026-725
Preprint. Discussion started: 18 September 2026

Column	Description	Unit
Day	Day of month	–
P	Daily precipitation	mm d^{-1}
ET_0	Daily reference evapotranspiration	mm d^{-1}

MFC2_SM_CRNS.csv provides the daily field-scale volumetric soil water content estimated from the calibrated Cosmic-Ray Neutron Sensor. The structure and variables included in this file are described in Table A2.3b.

Table A2.3b. Variables, descriptions, and units included in the MFC2_SM_CRNS.csv file

Column	Description	Unit
Year	Calendar year	–
Month	Calendar month	–
Day	Day of month	–
θCRNS	Field-scale volumetric soil water content	cm^3 cm^{-3}

MFC2_SM_z15cm.csv and MFC2_SM_z30cm.csv contain the daily average volumetric soil water content measured by the twenty GS3 sensors installed at depths of 15 cm and 30 cm, respectively. Each file includes the date (Year, Month, Day) followed by twenty columns corresponding to the individual SoilNet monitoring units (Units 1–20), reporting calibrated volumetric soil water content (θ, cm^3 cm^{-3}).

MFC2_TDR_SM.xlsx contains the campaign-based soil moisture surveys conducted using a portable time-domain reflectometer (TDR). The dataset comprises measurements collected during 19 sampling campaigns conducted between 4 October 2018 and 16 December 2021 at the 20 SoilNet monitoring locations. Each row corresponds to a sampling location, identified by its spatial coordinates, whereas the soil moisture observations from the 19 sampling campaigns are organized in separate columns, each identified by the corresponding sampling date. The structure and variables included in the file are described in Table A2.3c.

Table A2.3c. Variables, descriptions, and units included in the MFC2_TDR_SM.xlsx file. Each row represents one of the 20 SoilNet monitoring locations, whereas the date-labelled columns contain volumetric soil water content measured during the 19 sampling campaigns.

https://doi.org/10.5194/essd-2026-725
Preprint. Discussion started: 18 September 2026

Earth System Science Data Discussions
Open Access

Column	Description	Unit
POSITION	Sampling point identifier	–
X	Easting coordinate	m
Y	Northing coordinate	m
2018-10-04 ... 2021-12-16	Volumetric soil water content measured during each field campaign	$cm^3\ cm^{-3}$

MFC2_POT_z15cm.csv and MFC2_POT_z30cm.csv contain the corresponding daily average soil matric potential (h, kPa) measured by the MPS-6 sensors installed at 15 cm and 30 cm depth. The file structure is identical to that adopted for soil moisture, with one column for the date and twenty columns representing the individual monitoring units.

MFC2_ISOTOPES.xlsx contains the stable water isotope observations collected during the fortnightly sampling campaigns. The structure and variables included in this file are described in Table A2.3d.

Table A2.3d. Variables, descriptions, and units included in the MFC2_ISOTOPES.xlsx file

Column	Description	Unit
Compartment	Water compartment (Rain, Soil, Stream, Groundwater, Xylem)	–
Year	Calendar year	–
Month	Calendar month	–
Day	Day of month	–
$\delta^{18}O$	Oxygen isotope composition	‰ (VSMOW)
$\delta^{2}H$	Hydrogen isotope composition	‰ (VSMOW)

For soil water observations, the compartment identifier specifies the sampling depth (15, 30, or 100 cm), while groundwater measurements are available only for the MFC2 site.

Three additional CSV files provide the soil physical, hydraulic, and spectral properties measured during the targeted soil sampling campaigns described in Sect. 4.2.7. MFC2_SOILNET_20_SOIL_PROPERTIES.csv contains the soil properties determined at the 20 SoilNet monitoring locations. The structure and variables included in this file are described in Table A2.3e.

Table A2.3e. Variables, descriptions, and units included in the MFC2_SOILNET_20_SOIL_PROPERTIES.csv file

https://doi.org/10.5194/essd-2026-725
Preprint. Discussion started: 18 September 2026

Column	Description	Unit
X	Easting coordinate (UTM)	m
Y	Northing coordinate (UTM)	m
sand	Sand content	%
silt	Silt content	%
clay	Clay content	%
BD	Oven-dry soil bulk density	g cm^{-3}
SOC	Soil organic carbon content	%
K_0	Saturated hydraulic conductivity	cm h^{-1}
$K_{s\text{-}n}$	Near-saturated hydraulic conductivity determined in the field using the mini-disk infiltrometer	cm h^{-1}

MFC2_GRID_124_SOIL_PROPERTIES.csv contains the soil properties determined at the 124 sampling locations distributed over MFC2 according to the 25 m regular grid. The structure and variables included in this file are described in Table A2.3f.

Table A2.3f. Variables, descriptions, and units included in the MFC2_GRID_124_SOIL_PROPERTIES.csv file

Column	Description	Unit
ID	Sample identifier	-
X	Easting coordinate (UTM)	m
Y	Northing coordinate (UTM)	m
sand	Sand content	%
silt	Silt content	%
clay	Clay content	%
BD	Oven-dry soil bulk density	g cm^{-3}
SOC	Soil organic carbon content	%

MFC2_GRID_124_SPECTRA.csv contains ID sample, X and Y coordinates, followed by 2,151 spectral reflectance columns, representing diffuse reflectance measured at wavelengths from 350 to 2,500 nm in the visible to shortwave-infrared (VNIR–SWIR) domain. Reflectance is dimensionless.

https://doi.org/10.5194/essd-2026-725
Preprint. Discussion started: 18 September 2026

Open Access Earth System Science Data Discussions

A2.3.1 MFC2 EMI sub-folder

The MFC2 EMI sub-folder contains seven CSV files corresponding to repeated electromagnetic induction (EMI) surveys conducted on 4 August 2020, 29 October 2020, 15 December 2020, 5 February 2021, 30 April 2021, 5 August 2021, and 16 December 2021. The surveys were performed using the GEM-2 SKI multifrequency electromagnetic induction sensor (Geophex Ltd., USA), as described in Sect. 4.2.4. Each CSV file contains the raw EMI measurements acquired during a single field campaign, with each row representing an individual measurement along the survey path.

The files share a common structure. The Line and Sample fields identify the acquisition line and the sequential measurement number within that line, respectively. The line numbering may restart within the same survey when data acquisition was paused and subsequently resumed and should therefore be regarded primarily as an acquisition identifier rather than as a unique spatial transect number. The X and Y columns provide the planimetric coordinates of each measurement in the WGS 84 / UTM zone 33N coordinate reference system, whereas GPSalt reports the elevation provided by the integrated GPS receiver. Because vertical GPS accuracy is lower than horizontal positioning accuracy, GPSalt should be considered an approximate elevation rather than a high-accuracy topographic measurement.

The Mark field records user-defined markers entered during acquisition to identify specific locations or changes along the survey path. Status reports the operating status of the instrument, whereas GPSStat provides an indicator of GPS positioning status/quality. Acquisition time is provided both as the instrument internal time in milliseconds (ms) and as clock time (hhmmss.sss). Because the reliability of the calendar date stored by the acquisition console could not be verified retrospectively, the survey date specified in the file name should be regarded as the authoritative acquisition date.

The PowerLn variable provides an indicator of ambient electromagnetic interference associated with electrical power-line frequencies (50/60 Hz). For each observation, the electromagnetic response is reported through the in-phase (I_...Hz) and quadrature (Q_...Hz) components, expressed in parts per million (ppm), at six operating frequencies: 425, 1,525, 5,325, 18,325, 63,025, and 92,775 Hz. The QSum field reports the sum of the quadrature responses across the operating frequencies and provides a synthetic indicator of the overall electromagnetic response. In general, the lower operating frequencies have greater sensitivity to deeper portions of the subsurface, whereas the higher frequencies are relatively more sensitive to shallow soil layers and to conductive objects located close to the instrument. The structure and variables included in the 7 CSV-files are described in Table A2.3.1a.

Table A2.3.1a. Variables, descriptions, and units included in the 7 CSV files in the MFC2_EMI sub-folder

Column	Description	Unit
Line	Acquisition line identifier	–
Sample	Sequential measurement identifier within acquisition line	–

Column	Description	Unit
X, Y	Measurement coordinates (WGS 84 / UTM zone 33N)	m
GPSalt	GPS-derived elevation	m
Mark	User-defined acquisition marker	–
Status	Instrument status indicator	–
GPSStat	GPS positioning status/quality indicator	–
Time[ms]	Internal acquisition time	ms
Time[hhmmss.sss]	Acquisition clock time	hhmmss.sss
PowerLn	Power-line electromagnetic interference indicator	instrument output
I_425Hz … I_92775Hz	In-phase EMI response at each operating frequency	ppm
Q_425Hz … Q_92775Hz	Quadrature EMI response at each operating frequency	ppm
QSum	Sum of quadrature responses across frequencies	ppm

A2.3.2 MFC2 ERT sub-folder

The MFC2 ERT sub-folder contains Electrical Resistivity Tomography (ERT) measurements acquired during two field campaigns conducted on 29 October 2020 and 5 August 2021. Four ERT profiles (PR01–PR04) were surveyed during each campaign, resulting in a total of eight profile datasets. Measurements were acquired using a Syscal Pro resistivity meter (IRIS Instruments, France) with a dipole–dipole configuration and a 1 m nominal electrode spacing. A skip-4 acquisition sequence was adopted, with four electrode positions separating the current and potential dipoles.
The original measurements were recorded in the proprietary binary Syscal Pro format and subsequently exported using Prosys software to produce the CSV files distributed in the repository. Each row of the CSV files represents an individual four-electrode measurement associated with a specific ABMN quadrupole, where A and B are the current-injection electrodes, and M and N are the potential electrodes. The structure and variables included in the 8 CSV-files are described in Table A2.3.2a.

Table A2.3.2a. Variables, descriptions, and units included in the 8 CSV files in the MFC2_ERT sub-folder

Column	Description	Unit
El-array	Electrode-array/configuration identifier	–
xA (m)	Longitudinal position of current electrode A	m

https://doi.org/10.5194/essd-2026-725
Preprint. Discussion started: 18 September 2026

Open Access Earth System Science Data Discussions

Column	Description	Unit
xB (m)	Longitudinal position of current electrode B	m
xM (m)	Longitudinal position of potential electrode M	m
xN (m)	Longitudinal position of potential electrode N	m
Rho (Ohm.m)	Apparent electrical resistivity calculated from the measured resistance and geometric factor	Ω m
Dev. Rho (%)	Relative dispersion/deviation of the apparent resistivity measurement, providing an indicator of measurement stability	%
SP (mV)	Self-potential measured during acquisition	mV
VMN (mV)	Potential difference measured between electrodes M and N	mV
IAB (mA)	Electrical current injected through electrodes A and B	mA
Time (ms)	Measurement/integration time	ms
Name	Profile/acquisition identifier	–
Date	Date and time recorded by the acquisition system	–

The survey geometry is represented using a local one-dimensional coordinate system along each ERT transect. Electrode positions extend from 1 to 96 m, whereas transverse and vertical coordinates were set to zero in the original acquisition geometry. The distributed CSV files therefore provide the longitudinal electrode positions rather than georeferenced coordinates.

Profiles longer than the 48-electrode physical array were acquired using a roll-along procedure. Successive array positions were partially overlapped to extend the ERT profile while maintaining continuous subsurface coverage and avoiding gaps in the resulting pseudosection. Consequently, some ABMN quadrupoles occur more than once in profiles extending beyond the initial 48-electrode layout. These repeated measurements are retained in the repository because they represent the original acquisition sequence and may also provide useful information for evaluating measurement repeatability.

The original Syscal format additionally contains information on the number of stacks, receiver channels, synchronization and validity flags, transmitter and receiver battery status, internal instrument temperature, overload conditions, and other instrumental parameters. It also accommodates induced-polarization (IP) measurements, including chargeability and IP time-window information. However, the present surveys were acquired for electrical resistivity only; consequently, the IP-related fields are empty or zero and are not included in the distributed CSV files.

A2.4 DEM_1m_MFC2 folder

https://doi.org/10.5194/essd-2026-725
Preprint. Discussion started: 18 September 2026

The DEM_1m_MFC2 folder contains a high-resolution Digital Terrain Model derived from UAV-LiDAR surveys. The dataset provides detailed characterization of surface morphology and microtopography and is intended to support hydrological modeling, terrain analysis, and integration with remote sensing observations.

The datasets have been formatted using widely adopted file formats to maximize interoperability with common scientific software. Variable names, measurement units, acquisition periods, and missing-data conventions are consistently documented to facilitate automated data processing and reproducible analyses. The modular organization of the repository also allows future releases to incorporate additional observations while preserving backward compatibility.

A2.5 GOR1 folder

The GOR1 folder contains continuous hydrometeorological observations with wireless sensor network measurements, field-scale soil moisture estimates derived from Cosmic-Ray Neutron Sensing (CRNS), and stable water isotope measurements. The datasets are organized into separate files according to the monitored variable.

GOR1_P_ET0.csv contains the daily observations of P and ET_0 associated with the weather station located at GOR1 site. The structure and variables included in this file are described in Table A2.5a.

Table A2.5a. Variables, descriptions, and units included in the GOR1_P_ET0.csv file

Column	Description	Unit
Year	Calendar year	–
Month	Calendar month	–
Day	Day of month	–
P	Daily precipitation	mm d^{-1}
ET_0	Daily reference evapotranspiration	mm d^{-1}

GOR1_SM_CRNS.csv provides the daily field-scale volumetric soil water content estimated from the calibrated Cosmic-Ray Neutron Sensor. The structure and variables included in this file are described in Table A2.5b.

Table A2.5b. Variables, descriptions, and units included in the GOR1_SM_CRNS.csv file

Column	Description	Unit
Year	Calendar year	–
Month	Calendar month	–

https://doi.org/10.5194/essd-2026-725
Preprint. Discussion started: 18 September 2026

Column	Description	Unit
Day	Day of month	–
θCRNS	Field-scale volumetric soil water content	$cm^3\ cm^{-3}$

GOR1_SM_z15cm.csv and GOR1_SM_z30cm.csv contain the daily average volumetric soil water content measured by the twenty GS3 sensors installed at depths of 15 cm and 30 cm, respectively. Each file includes the date (Year, Month, Day) followed by twenty columns corresponding to the individual SoilNet monitoring units (Units 1–20), reporting calibrated volumetric soil water content (θ, $cm^3\ cm^{-3}$).

GOR1_TDR_SM.xlsx contains the campaign-based soil moisture surveys conducted using a portable time-domain reflectometer (TDR). The dataset comprises measurements collected during 16 sampling campaigns conducted between 14 November 2018 and 17 December 2021 at the 20 SoilNet monitoring locations. Each row corresponds to a sampling location, identified by its spatial coordinates, whereas the soil moisture observations from the 16 sampling campaigns are organized in separate columns, each identified by the corresponding sampling date. The structure and variables included in the file are described in Table A2.5c.

Table A2.5c. Variables, descriptions, and units included in the GOR1_TDR_SM.xlsx file. Each row represents one of the 20 SoilNet monitoring locations, whereas the date-labelled columns contain volumetric soil water content measured during the 16 sampling campaigns.

Column	Description	Unit
POSITION	Sampling point identifier	–
X	Easting coordinate	m
Y	Northing coordinate	m
Z	Elevation	m a.s.l.
2018-11-14 ... 2021-12-17	Volumetric soil water content measured during each field campaign	$cm^3\ cm^{-3}$

GOR1_POT_z15cm.csv and GOR1_POT_z30cm.csv contain the corresponding daily average soil matric potential (h, kPa) measured by the MPS-6 sensors installed at 15 cm and 30 cm depth. The file structure is identical to that adopted for soil moisture, with one column for the date and twenty columns representing the individual monitoring units.

https://doi.org/10.5194/essd-2026-725
Preprint. Discussion started: 18 September 2026

GOR1_ISOTOPES.xlsx contains the stable water isotope observations collected during the fortnightly sampling campaigns. The structure and variables included in this file are described in Table A2.5c.

Table A2.5c. Variables, descriptions, and units included in the GOR1_ISOTOPES.xlsx file

Column	Description	Unit
Compartment	Water compartment (Rain, Soil, Stream, Xylem)	–
Year	Calendar year	–
Month	Calendar month	–
Day	Day of month	–
$\delta^{18}O$	Oxygen isotope composition	‰ (VSMOW)
$\delta^{2}H$	Hydrogen isotope composition	‰ (VSMOW)

A2.5.1 GOR1 EMI sub-folder

The GOR1 EMI sub-folder contains five CSV files corresponding to repeated electromagnetic induction (EMI) surveys conducted on 14 December 2020, 4 February 2021, 29 April 2021, 6 August 2021, and 17 December 2021. All EMI files share the same data structure as those in MFC2, with each row representing an individual measurement acquired along the survey path. The Line and Sample fields identify the acquisition line and sequential measurement, while X and Y provide the planimetric coordinates and GPSalt the GPS-derived elevation. The fields Mark, Status, and GPSStat provide acquisition markers and information on instrument and GPS status, whereas acquisition time is reported as both internal time and clock time. PowerLn provides an indicator of ambient electromagnetic interference associated with electrical power lines. The electromagnetic response is reported as in-phase (I) and quadrature (Q) components, expressed in ppm, at six operating frequencies (425, 1,525, 5,325, 18,325, 63,025, and 92,775 Hz), while QSum represents the sum of the quadrature responses across frequencies.

A2.5.2 GOR1 ERT sub-folder

The GOR1 ERT folder contains Electrical Resistivity Tomography (ERT) data acquired during two field campaigns conducted on 14 December 2020 and 29 April 2021. Four profiles (PR01–PR04) were surveyed during each campaign, resulting in eight CSV files. The measurements were acquired using a Syscal Pro resistivity meter (IRIS Instruments, France) and subsequently exported from the original proprietary format. Each CSV file contains 2,207 records, with each row representing an individual

https://doi.org/10.5194/essd-2026-725
Preprint. Discussion started: 18 September 2026

Open Access Earth System Science Data Discussions

measurement associated with a specific four-electrode (ABMN) configuration. The structure and variables included in the 8 CSV-files are described in Table A2.5.2a.

Table A2.5.2a. Variables, descriptions, and units included in the 8 CSV files in the GOR1_ERT sub-folder

CSV field	Description	Unit
El-array	Electrode-array/configuration identifier	–
Spa.1	Longitudinal position of current electrode A	m
Spa.2	Longitudinal position of current electrode B	m
Spa.3	Longitudinal position of potential electrode M	m
Spa.4	Longitudinal position of potential electrode N	m
Rho	Apparent electrical resistivity calculated for the ABMN configuration	Ω m
Dev.	Measurement deviation, providing an indicator of measurement stability/quality	%
M	Induced-polarization/chargeability field	–
Sp	Self-potential	mV
Vp	Potential difference measured between electrodes M and N	mV
In	Electrical current injected through electrodes A and B	mA

The M field is equal to zero throughout these datasets because the surveys were conducted for electrical resistivity rather than induced polarization. The first column (Unnamed: 0) is empty in all files and results from the CSV export procedure; it contains no measurement information and should be ignored during data processing.

The electrode geometry is expressed using a local one-dimensional coordinate system along each ERT profile, rather than geographical coordinates. Spa.1–Spa.4 identify the longitudinal positions of electrodes A, B, M, and N, respectively. For example, the first record in all profiles corresponds to A = 1 m, B = 6 m, M = 2 m, and N = 7 m. Profiles were acquired using a roll-along procedure with partial overlap between successive electrode-array positions to extend the investigated transect while maintaining continuous subsurface coverage. Consequently, repeated ABMN configurations may occur in the files and have been retained as part of the original measurements.

Author contribution

Conceptualization and formal analysis: NR, PN. Data curation: All authors. Formal analysis: NR, GC, MC, CM, BS, UL, PN. Funding acquisition: NR, HV, GA, EBD, ChM, PN. Investigation: All authors.
Methodology: NR, HV, HRB, GC, GA, EBD, JM, PN. Project administration: NR, PN.
Resources: NR, HV, GA, ChM, CM, BS, UL, PN. Supervision: NR, HV, HRB, GC, GA, MP, LdS, PN.
Validation: All authors. Visualization: NR, GC, MC, NF, JM, PN.
Writing (original draft preparation) NR, PN. Writing (review and editing): All authors.

Competing interests

The authors declare that they have no conflict of interest

Disclaimer

Copernicus Publications adds a standard disclaimer: "Copernicus Publications remains neutral with regard to jurisdictional claims made in the text, published maps, institutional affiliations, or any other geographical representation in this paper. While Copernicus Publications makes every effort to include appropriate place names, the final responsibility lies with the authors. Views expressed in the text are those of the authors and do not necessarily reflect the views of the publisher."
Please feel free to add disclaimer text at your choice, if applicable.

Acknowledgments

The TERENO infrastructure in the Alento CZO was supported by the Helmholtz Association, the German Federal Ministry of Science, Technology and Space, and the Forschungszentrum Jülich GmbH. Maintenance activities, implementation of new infrastructures, sampling campaigns, and laboratory experiments were supported by the Italian team through the following projects: MiUR-PRIN Project "WATer mixing in the critical ZONe: observations and predictions under environmental changes – WATZON" (Grant 2017SL7ABC), WaterJPI2018 Closing the Water Cycle Gap Project "*iAqueduct – An integrative information aqueduct to close the gaps between global satellite observation of water cycle and local sustainable management of water resources*" (Project No.: ENWWW.2018.5), and MiUR-PNRR-PRIN Project "ASAP – Assessing and mapping novel agroecosystem vulnerability and resilience indicators in southern Italy" (Grant P2022-8L3KX). The authors also received support from the Deutsche Forschungsgemeinschaft (DFG, German Research Foundation), Project 357874777 of the research unit FOR 2694 Cosmic Sense, Next Generation EU - Italian NRRP, Mission 4, Component 2, Investment 1.5, call for the creation and strengthening of 'Innovation Ecosystems', building 'Territorial R&D Leaders' (Directorial Decree n. 2021/3277) - project Tech4You - Technologies for climate change adaptation and quality of life improvement, n. ECS0000009.

References

Ali, E., Cramer, W., Carnicer, J., Georgopoulou, E., Hilmi, N.J.M., Le Cozannet, G., and Lionello, P.: Cross-Chapter Paper 4: Mediterranean Region. In: Climate Change 2022: Impacts, Adaptation and Vulnerability. Contribution of Working Group II to the Sixth Assessment Report of the Intergovernmental Panel on Climate Change [H.-O. Pörtner, D.C. Roberts, M. Tignor, E.S. Poloczanska, K. Mintenbeck, A. Alegría, M. Craig, S. Langsdorf, S. Löschke, V. Möller, A. Okem, B. Rama (eds.)]. Cambridge University Press, Cambridge, UK and New York, NY, USA, pp. 2233–2272, doi:10.1017/9781009325844.021, 2022.

Allen, R.G., L.S. Pereira, D. Raes, and M. Smith. Crop evapotranspiration: guidelines for computing crop water requirements. Irrigation and Drainage Paper No. 56. 300 p. Food and Agriculture Organization of the United Nations (FAO), Rome, Italy, 1998

Auerswald, K., Geist, J., Quinton, J.N., and Fiener, P.: HESS Opinions: Floods and droughts – Land use, soil management, and landscape hydrology are more significant drivers than increasing temperatures, EGUsphere, 1702, doi:10.5194/egusphere-2024-1702, 2024.

Bates, B.C., Kundzewicz, Z.W., Wu, and S. Palutikof, J.P. (Eds.): Climate Change and Water. Technical Paper VI of the Intergovernmental Panel on Climate Change, IPCC Secretariat, Intergovernmental Panel on Climate Change, Geneva, 210 pp., ISBN:978-92-9169-123-4, 2008.

Batsukh, K., Zlotnik, V.A., Suyker, A., and Nasta, P.: Prediction of biome-specific potential evapotranspiration in Mongolia under a scarcity of weather data, Water, 13, 2470, doi:10.3390/w13182470, 2021.

Ben Dor, E., Granot, A., Wallach, R., Francos, N., Pearlstein, D.H., Efrati, B., Borůvka, L., Gholizadeh, A., Schmid, T.: Exploitation of the SoilPRO® (SP) apparatus to measure soil surface reflectance in the field: Five case studies, Geoderma,, 438, 116636, https://doi.org/10.1016/j.geoderma.2023.116636, 2023.

Blanchy G., S. Saneiyan, J. Boyd, P. McLachlan, and A. Binley: ResIPy, an intuitive open source software for complex geoelectrical inversion/modeling, Comput. Geosci., 137, 104423, 10.1016/j.cageo.2020.104423, 2020.

Bogena, H.R., Schrön, M., Jakobi, J., Ney, P., Zacharias, S., Andreasen, M., Baatz, R., Boorman, D., Duygu, M.B., Eguibar-Galán, M.A., Fersch, B., Franke, T., Geris, J., González Sanchis, M., Kerr, Y., Korf, T., Mengistu, Z., Mialon, A., Nasta, P., Nitychoruk, J., Pisinaras, V., Rasche, D., Rosolem, R., Said, H., Schattan, P., Zreda, M., Achleitner, S., Albentosa-Hernández, E., Akyürek, Z., Blume, T., del Campo, A., Canone, D., Dimitrova-Petrova, K., Evans, J.G., Ferraris, S., Frances, F., Gisolo, D., Güntner, A., Herrmann, F., Iwema, J., Jensen, K.H., Kunstmann, H., Lidón, A., Looms, M.C., Oswald, S., Panagopoulos, A., Patil, A., Power, D., Rebmann, C., Romano, N., Scheiffele, L., Seneviratne, S., Weltin, G., and Vereecken, H.: COSMOS-Europe: a European network of cosmic-ray neutron soil moisture sensors. Earth System Science Data, 14, 1125–1151, https://doi.org/10.5194/essd-14-1125-2022, 2022

Brisson, N., Gate, P., Gouache, D., Charmet, G., Oury, F.-X., and Huard, F.: Why are wheat yields stagnating in Europe? A comprehensive data analysis for France, Field Crops Research, 119, 201-212, doi:10.1016/j.fcr.2010.07.012, 2010.

Brooks, P. D., Chorover, J., Fan, Y., Godsey, S.E., Maxwell, R. M., McNamara, J. P., and Tague, C.: Hydrological partitioning in the critical zone: Recent advances and opportunities for developing transferable understanding of water cycle dynamics, Water Resour. Res., 51, 6973–6987, 2015.

Cassiani, G., Bruno, V., Villa, A., Fusi, N., and Binley A.M.: A saline tracer test monitored via time-lapse surface electrical resistivity tomography, *Journal of Applied Geophysics*, 59, 244-259, doi: 10.1016/j.jappgeo2005.10.007, 2006.

Desilets, D., Zreda, M., and Ferré, T. P. A.: Nature's neutron probe: Land surface hydrology at an elusive scale with cosmic rays, Water Resources Research, 46, https://doi.org/10.1029/2009WR008726, 2010.

Ellison, D., Futter, M.N., and Bishop, K.: On the forest cover-water yield debate: from demand- to supply-side thinking, Glob. Chang. Biol., 18, 806-820, 2012.

European Commission: Directorate-General for Research and Innovation, EU mission, a soil deal for Europe, Publications Office of the European Union, 2025, https://data.europa.eu/doi/10.2777/4948116

FAO-ITPS: Towards a definition of soil health, Soil Letters, 1, 2020.

Finley, A., Banerjee, S., and Hjelle, Ø.: MBA: Multilevel B-Spline Approximation. R package version 0.1-2, https://CRAN.R-project.org/package=MBA, 2024.

Francos, N., Romano, N., Nasta, P., Zeng, Y., Szabó, B., Manfreda, S., Ciraolo, G., Mészáros, J., Zhuang, R., Su, B., Ben-Dor, E.: Mapping water infiltration rate using ground and UAV hyperspectral data: A case study over Alento, Italy, Remote Sens., 13, 2606, 1-30, doi:10.3390/rs13132606, 2021.

Gee, G.W. and Or, D.: Particle-size analysis: hydrometer method. In "Methods of Soil Analysis: Part 4 - Physical Methods" (Dane, J.H., Topp, G.C., eds.), SSSA Book Series 5, Madison, USA, pp. 278-283, 2002.

Grant, G.E. and Dietrich, W.E.: The frontier beneath our feet, Water Resour. Res., 53, 2605-2609, doi:10.1002/2017WR020835, 2017.

Gaillardet, J., Braud, I., Hankard, F., Anquetin, S. et al.: OZCAR: The French network of critical zone observatories, Vadose Zone Journal, 17, 180067, doi:10.2136/vzj2018.04.0067, 2018.

https://doi.org/10.5194/essd-2026-725
Preprint. Discussion started: 18 September 2026

Heidbüchel, I., A. Güntner, and T. Blume: Use of cosmic-ray neutron sensors for soil moisture monitoring in forests. Hydrology and Earth System Sciences, vol. 20, pp. 1269-1288, 2016.

Horsburgh, J.S., Lehnert, K., Read, J., et al.: Lessons learned from developing and operating the Critical Zone Collaborative Network (CZNet) data cyberinfrastructure, Authorea, doi:10.22541/essoar.173457141.17661792/v1, 2024.

Köhli, M., Weimar, J., Schrön, M., Baatz, R., and Schmidt, U.: Soil Moisture and Air Humidity Dependence of the Above-Ground Cosmic-Ray Neutron Intensity, Frontiers in Water, 2, https://doi.org/10.3389/frwa.2020.544847, 2021.

Kutiel, H., Trigo, R.M.: The rainfall regime in Lisbon in the last 150 years, Theor Appl Climatol, 118, 387-403, doi:10.1007/s00704-013-1066-y, 2014.

IPCC: Climate Change 2022: Impacts, Adaptation and Vulnerability. Contribution of Working Group II to the Sixth Assessment Report of the Intergovernmental Panel on Climate Change [H.-O. Pörtner, D.C. Roberts, M. Tignor, E.S. Poloczanska, K. Mintenbeck, A. Alegría, M. Craig, S. Langsdorf, S. Löschke, V. Möller, A. Okem, B. Rama (eds.)]. Cambridge University Press. Cambridge University Press, Cambridge, UK and New York, NY, USA, 3056 pp., doi:10.1017/9781009325844, 2022

Lappalainen, H. K., Baklanov, A., Bäck, J., Arvanitidis, C., Basart, S., Bernier, N., et al.: Towards a Global Ground-Based Earth Observatory (GGBEO): Leveraging existing systems and networks. Big Earth Data, 1-36. https://doi.org/10.1080/20964471.2025.2574174, 2025.

Lazzaro U., Mazzitelli, C., Sica, B., Di Fiore, P., Romano, N., Nasta, P.: On evaluating the hypothesis of shape similarity between soil particle-size distribution and water retention function. J Agr Eng 54(4), https://doi.org/10.4081/jae.2023.1542, 2023.

Lee, S., Wolberg, G., and Shin, S. Y.: Scattered data interpolation with multilevel B-splines, IEEE Trans. Vis. Comput. Graph., 3, 228–244, https://doi.org/10.1109/2945.620490, 1997.

McLachlan, P., Blanchy, G., and Binley A.M.: EMagPy: Open-source standalone software for processing, forward modeling and inversion of electromagnetic induction data, Computers and Geosciences, 146, 104561, doi:10.1016/j.cageo.2020.104561, 2021.

Mebius, L.J.: A rapid method for the determination of organic carbon in soil. Anal. Chim. Acta. 22: 120–124, 1960

Nasta, P., Allocca, C., Deidda, R., and Romano, N.: Assessing the impact of seasonal-rainfall anomalies on catchment-scale water balance components, Hydrol. Earth Syst. Sci., 24, 1-17, doi:10.5194/hess-24-3211-2020, 2020a.

Nasta P., N. Romano, G.B. Chirico. Functional evaluation of a simplified scaling method for assessing the spatial variability of the soil hydraulic properties at hillslope scale. Hydrological Sciences Journal 58 (5): 1-13, 2013

Nasta, P., Bogena, H.R., Weuthen, A., Sica, B., Vereecken, H., and Romano, N.: Integrating invasive and non-invasive monitoring sensors to detect field-scale soil hydrological behavior, Front. Water, 2, 26, doi:10.3389/frwa.2020.00026, 2020b.

Nasta, P., Blöschl, G., Bogena, H.R., Zacharias, S., Baatz, R., De Lannoy, G., Jensen, K.H., Manfreda, S., Pfister, L., Tarquis, A.M., van Meerveld, I., Voltz, M., Zeng, Y., Kustas, W., Li, X., Vereecken, H., and Romano, N.: HESS Opinions: Towards a common vision for the future of hydrological observatories. Hydrol. Earth Sys. Sci. 29, 465-483, doi:10.5194/hess-29-465-2025, 2025.

Nasta P., Coccia, F., Lazzaro, U., Bogena, H.R., Huisman, A., Sica, B., Mazzitelli, C., Vereecken, H., and Romano, R.: Temperature-corrected calibration of GS3 and TEROS-12 soil water content sensors. Sensors 24, 952. https://doi.org/10.3390/s24030952, 2024.

Nasta, P., Palladino, M., Ursino, N., Saracino, A., Sommella, A., and Romano, N.: Assessing long-term impact of land use change on hydrologic ecosystem functions in a Mediterranean upland agro-forestry catchment, Sci. Total Environ., 605-606, 1070-1082, doi:10.1016/j.scitotenv.2017.06.008, 2017.

Nasta, P., Mazzitelli, C., Ben Dor, E., Romano, N. From light scan to flow: Estimating soil hydraulic properties through VNIR-SWIR spectroscopy and calibration-free PTFs. Eur J Soil Sci 77, 4: e70383. https://doi.org/10.1111/ejss.70383, 2026.

Nimmo, J.R. and Voss, P.R.: Improved calculation of hydraulic conductivity for small disk tension infiltrometers, Water Resour. Res., 59, 1-16, doi: 10.1029/2022WR032475, 2023.

Olson, K.R., Al-Kaisi, M., Lal, R., and Cihacek, L.: Impact of soil erosion on soil organic carbon stocks, J. Soil Water Conserv., 71:3, 61A-67A, doi: 10.2489/jswc.71.3.61A, 2016.

Peel, M.C., Finlayson, B.L., and McMahon, T.A.: Updated world map of the Köppen-Geiger climate classification, Hydrol. Earth Syst. Sci. 11, 1633–1644. https://doi.org/10.5194/hess-11-1633-2007, 2007.

https://doi.org/10.5194/essd-2026-725
Preprint. Discussion started: 18 September 2026

Romano, N. and Santini, A.: Determining soil hydraulic functions from evaporation experiments by a parameter estimation approach: Experimental verifications and numerical studies. Water Resour. Res. 35, 3343-3359, doi:10.1029/1999WR900155, 1999.

Romano, N. and Ursino, N.: Forest fire regime in a Mediterranean ecosystem: unraveling the mutual interrelations between rainfall seasonality, soil moisture, drought persistence, and biomass dynamics, Fire 3, 49, 1-19, doi:10.3390/fire3030049, 2020.

Romano, N., Mazzitelli, C., and Nasta, P.: Root-zone water-storage capacity and uncertainty: An intrinsic factor affecting agroecosystem resilience to drought. Water Resour. Res. 61, e2024WR037719, doi:10.1029/2024WR037719, 2025.

Romano, N., Nasta, P., Severino, G., and Hopmans, J.W.: Using bimodal log-normal functions to describe soil hydraulic properties, Soil Sci. Soc. Am. J. 75, 468-480, doi:10.2136/sssaj2010.0084, 2011.

Romano N., Nasta, P., Bogena, H.R., De Vita, P., Stellato, L., and Vereecken, H.: Monitoring hydrological processes for land and water resources management in a Mediterranean ecosystem: The Alento River catchment observatory, Vadose Zone J., 17, 80042. doi:10.2136/vzj2018.03.0042, 2018.

Romano, N., Vereecken, H., Bogena, H.R., Cassiani, G., Censini, M., Armiento, G., Proposito, M., De Silvestri, L., Ben Dor, E., Francos, N., Massari, C., Mészáros, J., Takáts, T., Mazzitelli, C., Sica, B. Lazzaro, U., and Nasta, P.: Complete dataset reflecting the spatial and thematic components of the Alento critical zone (CZ) observatory, https://doi.org/10.6084/m9.figshare.31229608, 2026.

Rosolem, R., Shuttleworth, W. J., Zreda, M., Franz, T. E., Zeng, X., and Kurc, S. A.: The effect of atmospheric water vapor on neutron count in the cosmic-ray soil moisture observing system, Journal of Hydrometeorology, 14, 1659–1671, https://doi.org/10.1175/JHM-D-12-0120.1, 2013.

Roussel, J.-R., Auty, D., Coops, N. C., Tompalski, P., Goodbody, T. R. H., Meador, A. S., Bourdon, J.-F., de Boissieu, F., and Achim, A.: lidR: An R package for analysis of Airborne Laser Scanning (ALS) data, Remote Sens. Environ., 251, 112061, https://doi.org/10.1016/j.rse.2020.112061, 2020.

Schaap, M.G., Leij, F.J.: Improved prediction of unsaturated hydraulic conductivity with the Mualem – van Genuchten model. Soil Sci Soc Am J 64, 843 – 851, 2000.

Su, Y., Besic, N., Zhang, X., Xu, Y., Francini, S., D'Amico, G., Chirici, G., Schwartz, M., Fayad, I., Brood, S., Pellissier-tanon, A., Yu, K., Chen, H., Chen, S., d'Aspremont, A., and Ciais, P.: A fused canopy height map of Italy (2004–2024) from spaceborne and airborne LiDAR, and Landsat via deep learning and Bayesian averaging, Earth Syst. Sci. Data Discuss. [preprint], https://doi.org/10.5194/essd-2025-378, in review, 2025.

Zacharias, S., Loescher, H.W., Bogena, H.R., Kiese, R., Schrön, M., Attinger, S., et al.: Fifteen years of integrated terrestrial environmental observatories (TERENO) in Germany: Functions, services, and lessons learned, Earth's Future, 12, e2024EF004510. https://doi.org/10.1029/2024EF004510, 2024

Zhang, K., Chen, S., Whitman, D., Shyu, M., Yan, J. and Zhang, C.: A progressive morphological filter for removing nonground measurements from airborne LIDAR data, IEEE Transactions on Geoscience and Remote Sensing, 41, 872–882, https://doi.org/10.1109/TGRS.2003.810682, 2003.

Zreda, M., Shuttleworth, W. J., Zeng, X., Zweck, C., Desilets, D., Franz, T., and Rosolem, R.: COSMOS: the COsmic-ray Soil Moisture Observing System, Hydrol. Earth Syst. Sci., 16, 4079–4099, https://doi.org/10.5194/hess-16-4079-2012, 2012.